iScience

CellPress
OPEN ACCESS

Article

Transgenic modeling of Ndr2 gene amplification reveals disturbance of hippocampus circuitry and function

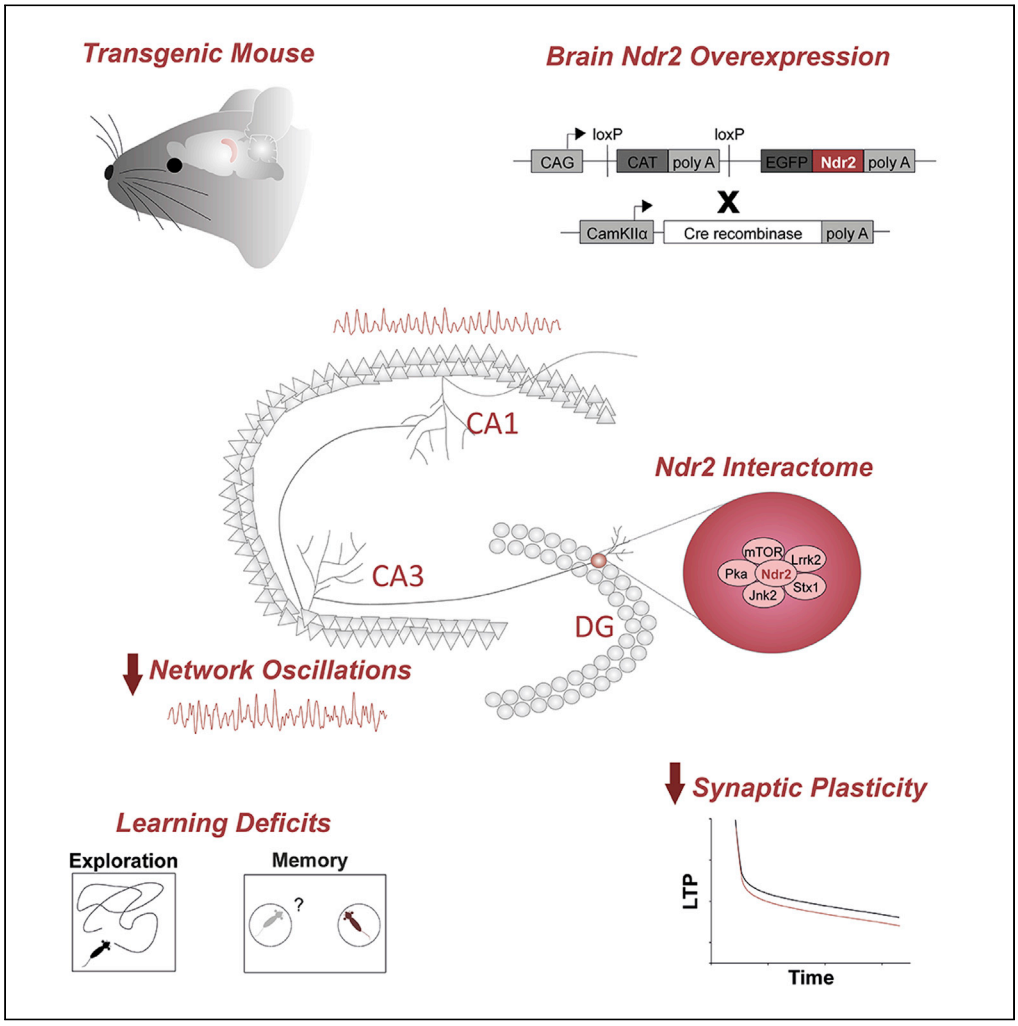

Deniz A. Madencioglu, Gürsel Çalışkan, Pingan Yuanxiang, ..., Thilo Kähne, Michael R. Kreutz, Oliver Stork

oliver.stork@ovgu.de

Highlights

Transgenic overexpression of Ndr2 in neurons impairs hippocampus-dependent behavior

Ndr2 gene amplification disturbs mossy fiber plasticity and CA3-CA1 network activity

Transgenic Ndr2 attenuates granule cell maturation and mossy fiber growth

Interactome analysis identifies Ndr2-related intracellular signaling pathways

Madencioglu et al., iScience 24, 102868
August 20, 2021
https://doi.org/10.1016/j.isci.2021.102868

iScience

CellPress
OPEN ACCESS

Article

Transgenic modeling of Ndr2 gene amplification reveals disturbance of hippocampus circuitry and function

Deniz A. Madencioglu,[1] Gürsel Çalışkan,[1,6] Pingan Yuanxiang,[2] Kati Rehberg,[1] Yunus E. Demiray,[1] Emre Kul,[1] Alexander Engler,[3] Hussam Hayani,[4] Jorge R. Bergado-Acosta,[1,6] Anne Kummer,[1] Iris Müller,[1,6] Inseon Song,[4] Alexander Dityatev,[4,6,7] Thilo Kähne,[3,6] Michael R. Kreutz,[2,5,6] and Oliver Stork[1,6,8,*]

SUMMARY

Duplications and deletions of short chromosomal fragments are increasingly recognized as the cause for rare neurodevelopmental conditions and disorders. The *NDR2* gene encodes a protein kinase important for neuronal development and is part of a microduplication region on chromosome 12 that is associated with intellectual disabilities, autism, and epilepsy. We developed a conditional transgenic mouse with increased Ndr2 expression in postmigratory forebrain neurons to study the consequences of an increased gene dosage of this Hippo pathway kinase on brain circuitry and cognitive functions. Our analysis reveals reduced terminal fields and synaptic transmission of hippocampal mossy fibers, altered hippocampal network activity, and deficits in mossy fiber-dependent behaviors. Reduced doublecortin expression and protein interactome analysis indicate that transgenic Ndr2 disturbs the maturation of granule cells in the dentate gyrus. Together, our data suggest that increased expression of Ndr2 may critically contribute to the development of intellectual disabilities upon gene amplification.

INTRODUCTION

The highly conserved Ndr (nuclear Dbf2-related) family of serine/threonine kinases is associated with the Hippo signaling pathway and involved in cellular functions ranging from cell division to polarized growth. Over recent years, evidence has accumulated that Ndr family kinases play important roles for nervous system development in both vertebrates and invertebrates (Emoto, 2011). In *Drosophilia melanogaster* the Ndr kinases Trc (Tricornered) and Fry (Furry) regulate dendritic branching and tiling, *i.e.*, the spatial separation of perceptive fields of neurons, by avoiding dendritic overlap (Emoto et al., 2004). Similarly, in *Caenorhabditis elegans*, their homolog SAX-1 (sensory axon guidance-1) together with SAX-2 regulates mechanosensory tiling by controlling the termination point of dendrites (Gallegos and Bargmann, 2004). In mammalian cells, two isoforms exist named Ndr1/2 (STK38, STK38L), which control dendrite growth and dendritic spine development (Rehberg et al., 2014; Ultanir et al., 2012). We have previously demonstrated that Ndr2, the predominant isoform in the mouse brain, interacts with the actin cytoskeleton and supports integrin-dependent neuronal differentiation in the primary neuron cultures (Rehberg et al., 2014; Stork et al., 2004). In fact, by controlling the distribution of specific integrin alpha/beta dimers in developing neurons, this kinase determines their response to different extracellular matrix components (Demiray et al., 2018). These functions also extend to neurite growth *in vivo* as observed in Ndr2-knockout mice, which show a transient overgrowth of basal dendrites and shortened primary branches of the apical dendrites of cornu ammonis (CA)3 pyramidal neurons in adulthood (Rehberg et al., 2014). We have previously observed induction of Ndr2 expression during fear memory consolidation (Stork et al., 2004), but the role of Ndr2 in information processing and cognitive functions has not been elucidated so far.

In humans, the *NDR2* gene is located on chromosome 12p11.23 and has been identified as part of a hotspot for microduplication bearing only three other genes (*ARNTL2*, *PPFIBP1*, and *SMCO2*) that are associated with reduced cognitive functioning, autism, or seizures in several individuals (Figure 1A and Table S1) (Firth

[1]Department of Genetics and Molecular Neurobiology, Institute of Biology, Otto-von-Guericke-University, 39120 Magdeburg, Germany

[2]Research Group Neuroplasticity, Leibniz Institute for Neurobiology, 39112Magdeburg, Germany

[3]Institute of Experimental Internal Medicine, Otto-von-Guericke-University, 39120Magdeburg, Germany

[4]Molecular Neuroplasticity Group, German Center for Neurodegenerative Diseases, 39120Magdeburg, Germany

[5]Leibniz Group 'Dendritic Organelles and Synaptic Function', University Medical Center Hamburg-Eppendorf, Center for Molecular Neurobiology, ZMNH, 20251Hamburg, Germany

[6]Center for Behavioral Brain Sciences, 39102Magdeburg, Germany

[7]Medical Faculty, Otto-von-Guericke-University, 39120Magdeburg, Germany

[8]Lead contact

*Correspondence: oliver.stork@ovgu.de

https://doi.org/10.1016/j.isci.2021.102868

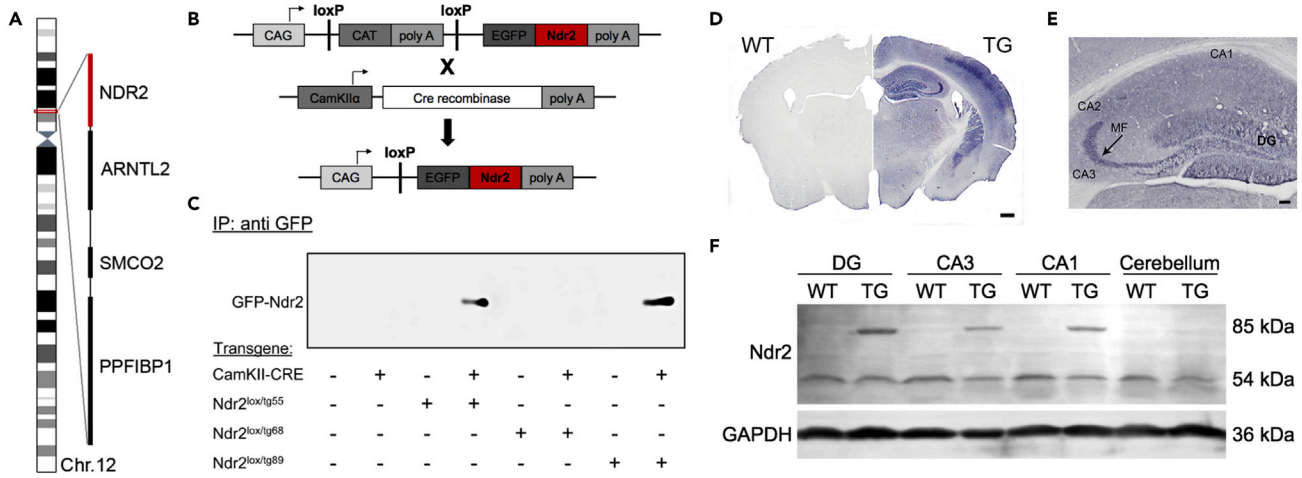

Figure 1. Generation and characterization of the Ndr2 overexpression in the forebrain of the transgenic mice

(A) Human chromosome 12, indicating four genes on the p arm between 12:27396901-27848497:1; NDR2 (STK38L), ARNTL2, SMCO2, and PPFIBP1.

(B) Our transgenic strategy comprises the generation of conditional EGFP:Ndr2-transgenic mice and their breeding with the CaMKII-alpha-Cre driver mice.

(C) Immunoprecipitation of EGFP:Ndr2 shows conditional expression in the brain of two mouse lines $Ndr2^{lox/tg55}$ and $Ndr2^{lox/tg89}$.

(D) An overview of coronal sections from WT and TG mouse brain tissues verifying the expression of the transgenic EGFP:Ndr2 in distinct regions of the brain of the TG mice by immunohistochemistry. Scale bar: 500 μm.

(E) In the hippocampus, prominent labeling of MF could be observed. Moderate staining was also observed in dendritic regions of DG and CA1. DG: Dentate gyrus, CA1-2-3: Cornu Ammonis 1-2-3, Shown with arrow MF: Mossy fibers. Scale bar: 500 μm.

(F) Ndr2 protein expression in the hippocampus (DG, CA3, and CA1) and cerebellum. The fusion protein could be detected at 85 kDa and through the molecular weight shift is discernible from endogenous Ndr2 in TG mice. The TG tissue sample from the cerebellum does not show a transgenic signal confirming the regional specificity of CaMKII-alpha-Cre mediated transgene activation.

See also Figure S1.

et al., 2009). Additionally, Pallister-Killian mosaic syndrome (PKS) (OMIM: #601803), a rare genetic disorder caused by a tetrasomy of chromosome 12p (Peltomäki et al., 1987), is characterized by multiple congenital anomalies including intellectual disabilities, but also facial dysmorphia, hypotonia, pigmentary dysplasia, seizures, diaphragmatic hernia, and congenital heart defects (Pallister et al., 1977; Schinzel, 1991; Teschler-Nicola and Killian, 1981). However, until now there are no suitable animal models available for these disorders, as in general there is a severe lack of animal models for rare neurodevelopmental disorders that arise from chromosomal rearrangement and copy number variation (see also, Hiroi and Yamauchi, 2019).

We hypothesized that the observed symptom manifestations of chromosome 12p11.23 microduplication and PKS involve a change in the function of Ndr2 and therefore tested whether an overexpression of the Ndr2 protein in mice may impair formation and function of neural circuits and thus contribute to the observed cognitive disturbances and/or autistic features. To this end, we generated and analyzed transgenic mice with an overexpression of Ndr2 in postmigratory forebrain neurons under the control of the promoter for calcium/calmodulin-dependent kinase II (CaMKII). This allowed us to target the cognitive functions of Ndr2 approximating the expression of endogenous Ndr2 in the mouse brain, which increases prominently during the third postnatal week, and can be found in principle neurons of adult hippocampus and neocortex (Stork et al., 2004; Rehberg et al., 2014; see also Figure S2 for mRNA levels in the hippocampus). A transgenic line was selected in which the transgene increased total levels of Ndr2 protein expression to almost two-fold of control levels in different hippocampal subregions (dentate gyrus, DG, and cornu ammonis 3, CA3). The transgene profoundly localized to hippocampal mossy fibers (MF), which are well suited to determine structure-function relationships and effects of genetic insults on cognitive brain function in mice (Berger et al., 2006; Dumas et al., 2004). We therefore determined in these transgenic mice the effect of Ndr2 overexpression on MF density and on the efficacy and plasticity at the MF-CA3 synapse. Furthermore, we began to address the underlying cellular processes and studied the consequences of altered MF function for behaviorally-relevant hippocampal network activity patterns and hippocampus-dependent learning and behavior. Collectively, our data provide evidence that increased expression of Ndr2 disturbs neuronal circuit formation and information processing in the hippocampus. We propose that transgenic overexpression of Ndr2 can be used to model network changes underlying the intellectual disability phenotype evoked by copy number variations of the NDR2 gene.

RESULTS

Transgenic mice overexpressing Ndr2 in the forebrain

We generated mice carrying a conditional transgenic EGFP:Ndr2 construct and subsequently crossed these with a driver mouse line expressing Cre recombinase under the CaMKII-alpha promoter. Thereby, we aimed to achieve CAG promoter-driven expression of EGFP:Ndr2 fusion protein in postmigratory neurons (Figure 1B). Previously, we have shown that the N-terminal addition of the EGFP tag does not interfere with the localization and function of Ndr2. We have shown that the EGFP:Ndr2 fusion protein localizes in the neurons and neuron-like cells in the same manner as endogenous Ndr2 (Stork et al., 2004) and, importantly, the expression of EGFP:Ndr2 in primary hippocampal neurons rescues the Ndr2-knockdown induced growth deficits in the dendrites and axons (Rehberg et al., 2014). After pronucleus injection of the EGFP:Ndr2 transgenic construct, we obtained several transgenic founders that were first bred with C57Bl/6 wild type mice to establish stable transgenic lines. Testing for genomic transgene insertion in F1, we identified three transgenic mouse lines designated $Ndr2^{lox/tg55}$ ($Tg(CAG\text{-}Egfp\text{:}Stk38l)55^{Stork}$), $Ndr2^{lox/tg68}$ ($Tg(CAG\text{-}Egfp\text{:}Stk38l)68^{Stork}$), and $Ndr2^{lox/tg89}$ ($Tg(CAG\text{-}Egfp\text{:}Stk38l)89^{Stork}$), according to the injection experiment. The genotypes of offspring from these lines and their intercross with CaMKII-alpha-Cre drivers were derived at Mendelian frequencies. The obtained transgenic mice were viable without overt morphological or behavioral phenotype.

Transgene expression in the brain was first verified with immunoprecipitation using anti-GFP antibodies for the precipitation and anti-Ndr2 for detection of the transgenic protein in western blots. Signals were obtained in lines $Ndr2^{lox/tg55}$ and $Ndr2^{lox/tg89}$ at the expected size of 85 kDa, representing the combined molecular weight of EGFP and Ndr2 (Figure 1C). Since the employed antibodies were directed to the N-terminal EGFP tag and the C-terminal proportion of Ndr2 (aa420-430(Stork et al., 2004)), we concluded the expression of full-length Ndr2 in these two lines. Moreover, no expression was observed in the absence of the Cre driver, demonstrating the specificity of the conditional expression. The numbers of transgene copies in the genomes of $Ndr2^{lox/tg55}$ and $Ndr2^{lox/tg89}$ transgenic mice were determined using a Ndr2 copy number assay, with non-transgenic littermates serving as controls. Our data indicate the existence of one supernumerous copy of Ndr2 in the genomic DNA of $Ndr2^{lox/tg55}$ mice and three additional copies in $Ndr2^{lox/tg89}$ mice (wild type control: 2.06 $\pm$ 0.06, $Ndr2^{lox/tg55}$: 2.98 $\pm$ 0.06, $Ndr2^{lox/tg89}$: 4.88 $\pm$ 0.015). Based on this characterization, we decided to use the $Ndr2^{lox/tg89}$ mouse line for further experiments. For simplicity, $Ndr2^{lox/tg89}$ x CaMKII-Cre mice are referred to as transgenic (TG) and their $Ndr2^{lox/tg89}$ littermate controls without the Cre activator as wildtype (WT).

TGNdr2 expression in the hippocampus

The expression and distribution of the transgenic Ndr2 in the brain was examined with immunohistochemistry using an anti-GFP antibody. Thereby, EGFP:Ndr2 could only be detected in the TG but not in WT mice (Figure 1D). Prominent transgene expression was observed in various forebrain regions including hippocampus and neocortex (mostly layer IV), striatum, thalamic nuclei, the amygdala, and the septum (S1 Fig), thus closely matching the expression pattern of CaMKII-alpha. Pronounced transgene expression in the hippocampus was observed, especially in the DG and the MF (Figure 1E). To quantify regional expression levels, western blotting was done with samples collected from the hippocampal subregions (DG, CA3, and CA1) and included cerebellum as a negative control. The 85 kDa fusion protein could be detected in all hippocampal subregions of TG but not WT mice, in addition to the signal of the endogenous Ndr2 at 54 kDa. By contrast, no transgene was detectable in the cerebellum, in line with the restriction of CaMKII-alpha driven Cre to the adult forebrain (Figure 1F). Quantification of immunoblot signals revealed that the total amount of Ndr2 (endogenous plus transgenic protein) in the hippocampal subregions of TG mice was clearly increased in the DG-CA3 system compared to the Ndr2 expression in corresponding regions of WT mice (Relative values of the total Ndr2 in TG to the endogenous Ndr2 in the WT mice: 1.955 $\pm$ 0.101 in DG, 1.819 $\pm$ 0.386 in CA3, 1.236 $\pm$ 0.093 in CA1; Relative values of endogenous Ndr2 in TG to endogenous Ndr2 in the WT mice: DG: 0.92 $\pm$ 0.07; CA3: 0.99 $\pm$ 0.09; CA1: 0.61 $\pm$ 0.05). In parallel, we determined the mRNA levels of Ndr2 and other core members of the Hippo signaling pathway in the granule cell layers in the DG of WT mice at P15, P30, and 3 months of age. Our data demonstrate that together with Ndr2 and its close homolog Ndr1, the Hippo kinases Mst2 and Mst3 as well as Lats1 and Lats2 are endogenously expressed in these cells. We further observed that endogenous Ndr2 is prominently regulated and increased in expression during postnatal development (Figure S2).

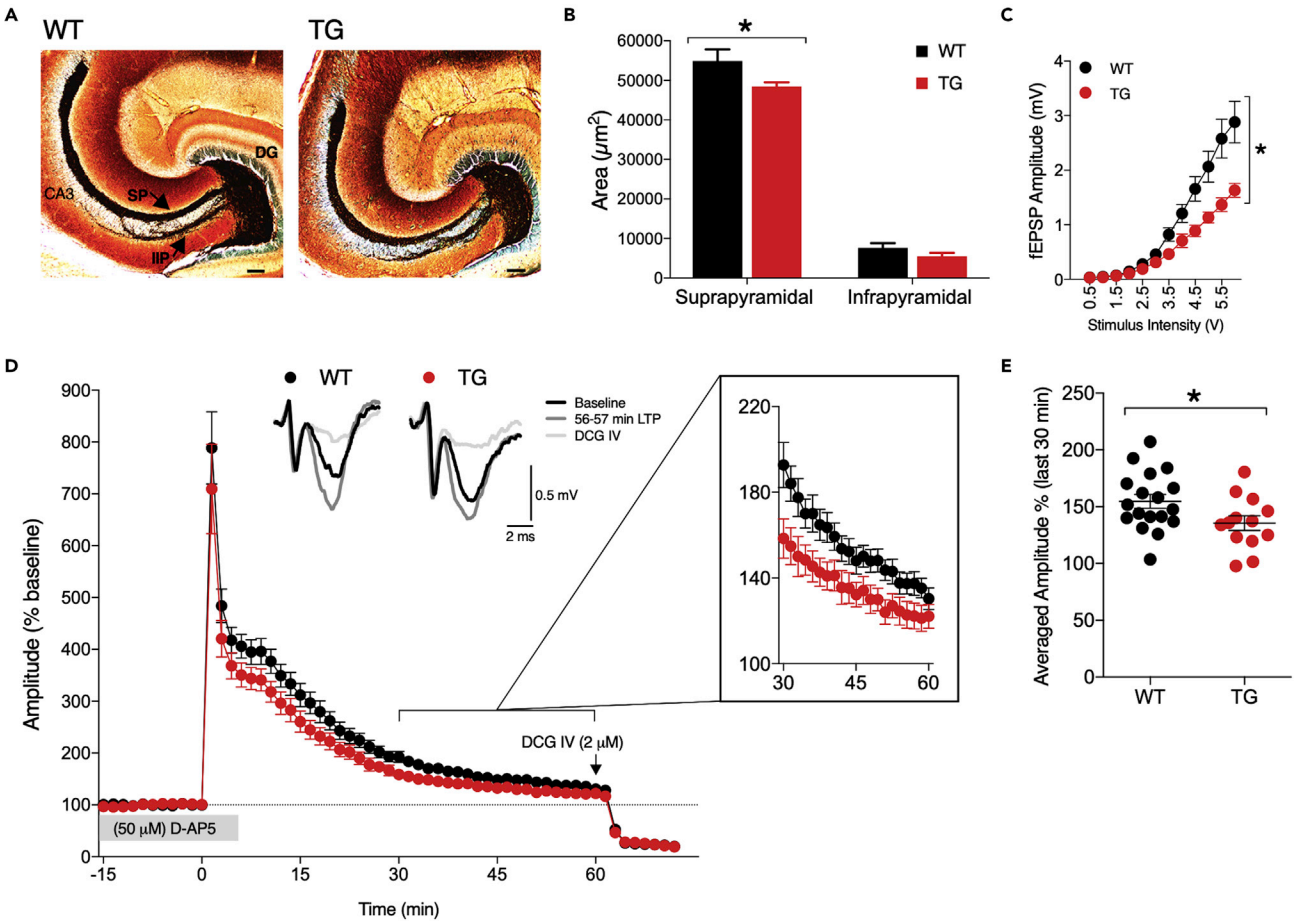

Figure 2. Reduced MF density, diminished basal transmission, and mildly decreased late MF-LTP in TG mice

(A) Representative images of the ventral DG and the MF from WT and TG mouse. Timm labeled mossy fibers are visible in black, with a pronounced suprapyramidal (SP) and discernable infra/intrapyramdial (IIP) band in both genotypes. Scale bar: 100 μm.

(B) Quantification of Timm labeling revealed a reduction in the ventral suprapyramidal mossy fiber band of TG mice (WT N = 5, TG N = 9). Values are mean ± SEM;* indicates $p < 0.05$

(C) Input/output ratios were significantly reduced in the TG mice indicating a decline in baseline synaptic responses (WT N = 5 mice, n = 18 slices, TG N = 4 mice, n = 13 slices). Values are mean ± SEM; *, $p < 0.05$

(D) Samples of MF-LTP traces during baseline recordings (black line); last minutes of LTP (gray line), and after DCG IV application (light gray line). The MF-LTP was induced by HFS in the presence of 50 μM D-AP5, and 2 μM DCG IV was applied to confirm the recorded fEPSPs as MF signals. Inset figure shows the last 30 min of the MF-LTP before DCG IV application.

(E) The column scatterplot of averaged fEPSP amplitudes from 30 min to 60 min after LTP induction. * indicates $p < 0.05$ by repeated measures two-wayANOVA in A and Student's t-test in E.

See also Figures S3–S5.

Reduction of mossy fibers in the ventral hippocampus of TG mice

To begin examining the putative effects of Ndr2 overexpression on MF, we next studied the MF using the Timm staining method (Figure 2A) and analyzed the size of the suprapyramidal and infrapyramidal bands. Overall, comparable structures of the hippocampal MF could be detected in the WT and TG mice and no signs of aberrant MF sprouting could be observed. However, a reduction in MF labeling became evident in the ventral suprapyramidal layer in the hippocampus of TG mice (Student's t-test, $t(12) = 2.505$, $p = 0.0276$ compared to WT mice) (Figure 2B). No quantitative change was observed in the ventral infrapyramidal band (Student's t-test, $t(12) = 1.454$, $p = 0.1716$) (Figure 2B) or in either bands in the dorsal hippocampus (Student's t-test, suprapyramidal: $t(14) = 0.5639$, $p = 0.5817$, infrapyramidal: $t(14) = 0.9991$, $p = 0.3347$) (Figure S4D). Black-Gold staining confirmed that fiber tracts throughout the brain did not show overt alterations as a result of the overexpression of Ndr2 (Figure S3). In summary, TG mice show quantitative reduction in ventral hippocampal MF.

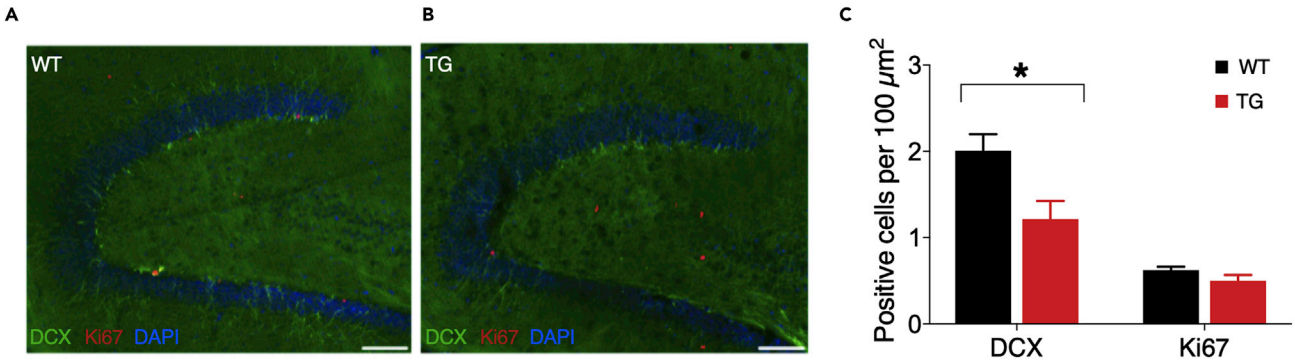

Figure 3. Disturbed MF maturation in TG mice

Expression of DCX (green) and Ki67 (red) in the vDG of a WT (A) and a TG (B) mouse. A reduced doublecortin labeling is evident along the entire extension of the DG granule cell layer. Bar, 100 μm (C) Quantification of DCX expressing cell profiles confirms the significant reduction, in the absence of a change in Ki67. Values are mean ± SEM; * indicates $p < 0.05$ for genotype.

See also Table S4.

Reduced synaptic transmission and LTP at the mossy fiber synapse of TG mice

We next assessed the synaptic transmission and plasticity in the MF-CA3 synapse to elucidate the impact of the identified MF phenotype. We observed that basal synaptic transmission at the ventral MF synapses was significantly reduced in TG mice as evident by the decreased fEPSP amplitudes (repeated measures two-wayANOVA, effect of genotype: $F(1,29) = 7.587$, $p = 0.0100$) (Figure 2C), across stimulus intensity levels. Moreover, a statistically significant interaction of genotype and stimulus intensity was found concerning fiber volley amplitudes (repeated measures two-wayANOVA: $F(11,319) = 1.982$, $p = 0.0296$), but the effect of genotype did not reach significance level ($F(1,29) = 2.769$, $p = 0.1069$) (Figure S4A). Based on this reduction in MF responsiveness, we next examined presynaptic short-term plasticity which, however, was not affected in the TG mice, since train facilitation (repeated measures two-wayANOVA, effect of genotype: $F(1,29) = 1.884$, $p = 0.1804$) and frequency facilitation ($F(1,29) = 0.2887$, $p = 0.5951$) (Figures S4B and S4C) were not different between genotypes. Finally, mossy fiber LTP (MF-LTP) was tested using a high frequency stimulation (HFS) protocol in the presence of 50 μM D-AP5 (Figure 2D). The initial potentiation during the HFS was not different between the genotypes (first 3 min after HFS: repeated measures two-wayANOVA, effect of genotype: $F(1,29) = 0.8454$, $p = 0.3654$), but the late phase (last 30 min) of this NMDAR-independent LTP was significantly reduced in the TG mice (planned comparison with Student's t-test, $t(29) = 2.133$, $p = 0.0415$) (Figure 2E). Together, these data reveal a functional deficit of the ventral hippocampal mossy fiber system in TG mice. Importantly, no comparable change in physiological properties could be observed in the dorsal hippocampal MF system (Figures S4E–S4J), and no change of basal synaptic transmission, short- or long-term plasticity was observed in area CA1 *stratum radiatum* in response to stimulation of Schaffer collaterals/commissural fibers of CA3 pyramidal cells (Figure S5).

Disturbed granule cell differentiation

To address potential mechanisms of disturbed mossy fiber plasticity in TG mice, we analyzed the expression of Ki67 as a marker for neurogenesis and doublecortin (DCX) as a marker of maturating granule cells in the adult dentate gyrus. Our data reveal a reduced number of doublecortin positive cells in the ventral hippocampus (Student's t-test: $t(12) = 2.787$, $p = 0.0164$), but no change in the number of Ki67 positive cells (Student's t-test: $t(13) = 1.670$, $p = 0.1187$) in 4-month-old TG mice compared to their WT littermates (Figure 3).

In order to identify putative cellular interaction partners of transgenic Ndr2 that may mediate its effect on these processes, we immunoprecipitated Ndr2-associated proteins from the adult TG hippocampus via the GFP tag of the transgene (Table S2). Annotation analysis of the obtained proteins suggests a predominant involvement in RNA processing, cytoskeleton organization, protein transport, and intracellular signaling/protein phosphorylation (Table S3). Further analyzing the identified proteins, we found 31 putative direct interaction partners of Ndr2 in these protein clusters, based on biochemical evidence from other species. Five of these (mTOR, PKA, Syntaxin1, Lrrk2, and JNK2) have previously been implicated in development

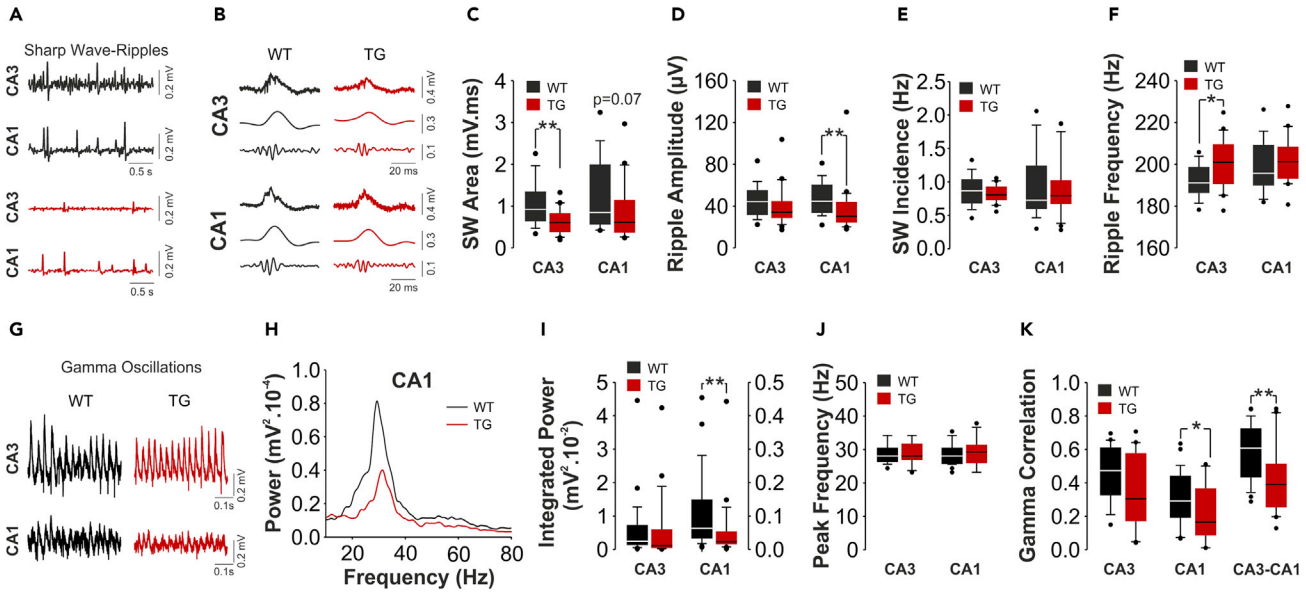

Figure 4. Reduced SW-R and carbachol-induced gamma oscillations in the ventral hippocampus of TG mouse

(A) Sample field potential (FP) traces simultaneously recorded from CA3 (upper trace) and CA1 (lower trace) subregions of the ventral-to-mid hippocampal slices from WT (black) and TG (red) mice.

(B) A sample sharp wave-ripple (SW-R; top trace) together with low-pass-filtered SW (3–45 Hz; middle trace) and band-passfiltered ripples (120–300 Hz; bottom trace) from CA3 and CA1 subregions of WT (black) and TG (red) slices. Note the reduced SW amplitude in CA3 subregion and reduced ripple amplitude in CA1 subregions in TG slices.

(C–F)(C) Summary graphs indicating a reduced SW area in the CA3 subregion of TG mice (WT: N = 5 mice, n = 22 slices; TG: N = 5 mice, n = 18 slices), (D) a reduced ripple amplitude in the CA1 subregion of TG slices, (E) no significant alterations in SW incidence in both CA3 and CA1 subregions and (F) a mild but significant increase in ripple frequency in the CA3 subregion of TG slices.

(G) Sample 5 μM carbachol-induced gamma oscillation field potential (FP) traces recorded from CA3 (top) and CA1 (bottom) subregions of the ventral-to-mid hippocampal slices of WT (black) and TG (red) mouse. Note the decreased gamma oscillation strength in the CA1 subregion of the TG mouse.

(H) Representative power spectra illustrating a general reduction in gamma oscillations in the CA1 subregion of a TG slice.

(I and J)(I) Summary graphs indicating a significant decrease in integrated gamma power (20–60 Hz) in the ventral CA1 subregion (WT: N = 5 mice, n = 29 slices; TG: N = 5 mice, n = 23 slices) and (J) no alteration in peak gamma frequency in both CA3 and CA1 subregions of TG slices (WT: N = 5 mice, n = 29 slices; TG: N = 5 mice, n = 23 slices).

(K) Summary graphs indicating a significant decrease in auto-correlation only in the CA1 subregion (WT: N = 5 mice, n = 28 slices; TG: N = 5 mice, n = 17 slices), no alteration in the CA3 subregion and a significant decrease in cross-correlation of gamma oscillations in the CA3 and CA1 subregion of the TG mice (WT: N = 5 mice, n = 29 slices; TG: N = 5 mice, n = 20 slices). All data are reported as box plots with the median value as the horizontal line. The boundary of the box closest to zero indicates the 25th percentile and the boundary of the box farthest from zero indicates the 75th percentile. Whiskers (error bars) above and below the box indicate the 90th and 10th percentiles. Data points (single dots) beyond the 5th and 95th percentiles are also displayed. *, ** indicate $p < 0.05$ and $p < 0.01$, respectively; Student's ttest (C: CA3; F: CA3, CA1; K: CA1, CA3-CA1) or Mann Whitney U test (C: CA1; D: CA3, CA1; E: CA3, CA1; I: CA3, CA1; J: CA3, CA1; K: CA3).

(Lrrk2), epilepsy-induced sprouting (mTor, JNK2), or presynaptic plasticity (Syntaxin 1, PKA) of MF (Table S4).

Reduced network oscillations in the ventral hippocampus of TG mice

To address the consequences of altered MF growth and function in TG mice, we then studied hippocampal network activities and hippocampus-dependent behavior. The ventral hippocampus is critical for the emergence of memory-related network oscillations *in vitro* and excitatory MF input to the ventral CA3 has been proposed to profoundly modulate this function (Rex et al., 2009; Sasaki et al., 2018). Specifically, under low cholinergic tonus (e.g., slow wave sleep), hippocampal CA3-CA1 axis generates local field potential (LFP) events called "sharp wave-ripple" (SW-R), during which learning-associated cellular activity patterns are reactivated, therefore, supporting the "offline" memory consolidation (Buzsáki, 2015; Wilson and McNaughton, 1994). Importantly, these SW-R events also occur spontaneously in slices obtained from ventral-to-mid portion of the hippocampus (Çalışkan et al., 2015a, 2016; Maier et al., 2003; Papatheodoropoulos and Kostopoulos, 2002). Indeed, we observed prominent SW-R both in CA3 and CA1 subregions in 40 slices out of 56 slices analyzed from both genotypes (Figures 4A and 4B). However, comparing various SW-R parameters

between genotypes, moderate changes were identified. Thus, a significant reduction in SW area (Figure 4C) in the CA3 subregion (Student's t-test: t(38) = -3.131, p = 0.003) and a tendency for a reduction in the CA1 subregion (Mann-Whitney U = 131, p = 0.071) were apparent in the TG mouse slices. Furthermore, the ripple amplitude (Figure 4D) was significantly decreased in the CA1 subregion (Mann-Whitney U = 93, p = 0.004), although not altered in the CA3 subregion (Mann-Whitney U = 145, p = 0.153). The incidence of SW (Figure 4E) did not change significantly in either CA3 (Mann-Whitney U = 174.0, p = 0.523) or CA1 (Mann-Whitney U = 187.5, p = 0.786) subregions of the TG mouse. Last, comparison of ripple frequencies (Figure 4F) revealed a significant increase only in the CA3 subregion (Student's t-test: CA3: t(38) = 2.376, p = 0.023; CA1: t(38) = -0.837, p = 0.408). Collectively, these data demonstrate that spontaneous SW-R activity is altered in the ventral hippocampus of TG mouse.

On the other hand, under increased cholinergic tonus, hippocampal CA3-CA1 circuits generate gamma oscillations both *in vitro* and *in vivo* (Vandecasteele et al., 2014; Zemankovics et al., 2013). Coherent LFP gamma oscillations in the hippocampal CA3-CA1 axis are associated with successful memory retrieval (Montgomery and Buzsáki, 2007). In addition, hippocampal gamma oscillation power is profoundly enhanced during episodes of high anxiety and emotional load (Çalışkan and Stork, 2019). Thus, we measured gamma oscillations induced by bath-application of cholinergic agonist Carbachol (CBh) to mimic high cholinergic hippocampal network state. To this end, slices were perfused with 5 μM CBh and 2 min LFP recordings were obtained after 50–70 min perfusion of CBh (Figure 4G). Here, genotype differences were most prominent in the CA1 subregion, where the integrated gamma power was significantly reduced in TG mice (Figures 4H and 4I; CA3: Mann-Whitney U = 254, p = 0.146; CA1: Mann-Whitney U = 184, p = 0.003). By contrast, the peak gamma frequency was not altered between the genotypes (Figure 4J; CA3: Mann-Whitney U = 315, p = 0.738; CA1: Mann-Whitney U = 325, p = 0.685). Correlation analysis indicated a significant decrease in auto-correlation of local gamma oscillations in the CA1 subregion (Figure 4K; CA3: Mann-Whitney U = 252, p = 0.136; CA1: Student's t-test t(43) = -2.135, p = 0.038) of the TG mice. This finding was accompanied by a significant reduction in cross-correlation between CA3 and CA1 gamma oscillations (Figure 4K; Student's t-test t(47) = -2.921, p = 0.005). No change in generation of recurrent epileptiform discharges (REDs) was evident upon CBh perfusion in the TG mouse slices in comparison to WT slices (WT: 0 out of 29 slices vs. TG: 3 out of 26 slices; Fisher exact test, p = 0.099). Together, these data describe reduced cholinergic gamma oscillations in the ventral hippocampus of the TG mice.

Learning impairments and increased exploratory behavior in TG mice

Finally, we aimed to evaluate putative behavioral consequences of the impaired hippocampal function. We found that home cage activity was not different between WT and TG mice (repeated measures two-way-ANOVA, effect of genotype: F(1,16) = 1.048, p = 0.3212) (Figure 5A) and TG mice exhibited normal activity during both the active and inactive phases of the day/night cycle. However, TG mice showed persistently increased levels of spatial exploration in the open field on both test days (day1: F(1,14) = 5.117, p = 0.0401, day 2: F(1,14) = 6.062, p = 0.0274) (Figure 5B). During the first test day, both WT and TG mice gradually habituated to the enclosure as the distance covered in the box slightly decreased over time. On the second day, activity levels remained largely unchanged within the observed time frame in both genotypes. No difference between genotypes was observed concerning the entries to the central compartment on either day (repeated measures two-wayANOVA, effect of genotype: day1: F(1,14) = 0.4816, p = 0.4990, day 2: F(1,13) = 0.0479, p = 0.8301). Thus, TG mice showed significantly increased exploration of a novel environment, but no change in exploratory pattern or habituation. In line with this, no change of anxiety-like behavior was observed in the dark-light transition test (Student's t-test: dark and light compartments: t(14) = 0.5655, p = 0.5807) or in the elevated plus maze (EPM) (Student's t-test: open arm entry %: t(14) = 1.027, p = 0.3219), total arm entries: t(14) = 0.7969, p = 0.4388 (Figure 5C); time spent in the open arms: WT = 43.84 ± 6.50 s, TG = 34.73 ± 6.75 s, t(14) = 0.9729, p = 0.3471).

MF-dependent learning was then assessed using an active avoidance paradigm. Over the five days of training, mice exhibited a learning curve increasing their performance to levels of 60–80% successful avoidance. However, TG mice increased their performance more slowly and reached only a lower level of successful avoidance compared to the WT group (repeated measures two-wayANOVA, effect of genotype: F(1,12) = 7.129, p = 0.0204), suggesting a learning impairment in this task (Figure 5D). Moreover, social memory was then investigated in a three-compartment test system. During the habituation phase, neither WT nor TG mice showed a preference for any side (Student's t-test: t(21) = 0.8312) and both groups displayed similar preference for the side that was baited with a partner mouse in the subsequent affiliation

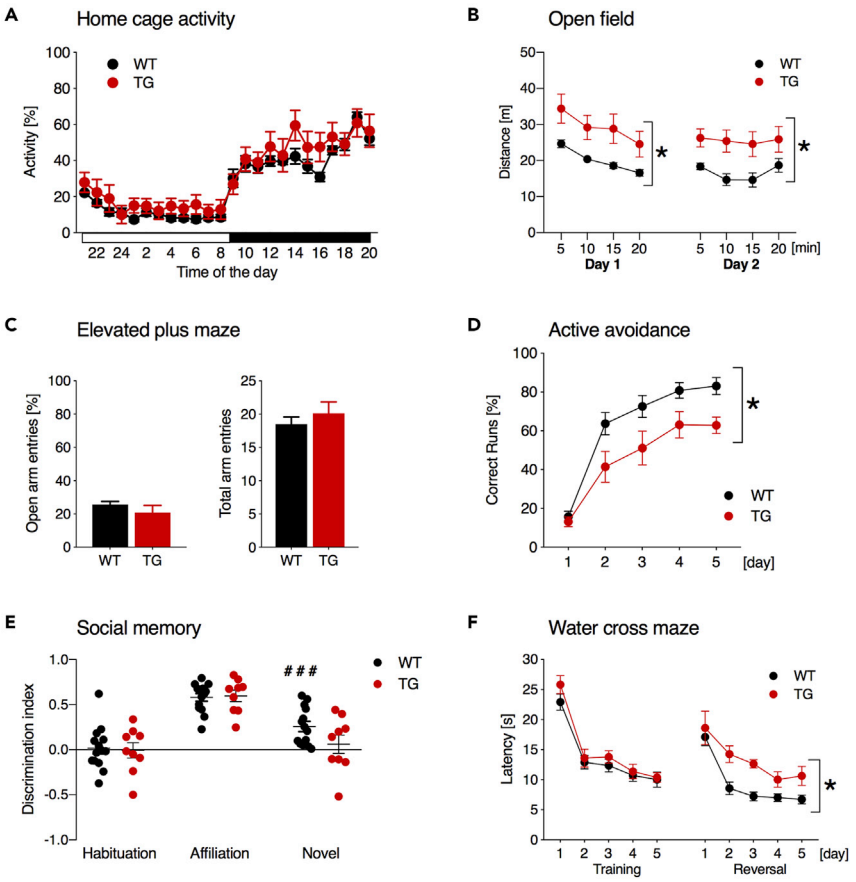

Figure 5. Increased exploratory activity and learning deficits in TG mice

(A) Activity in the home cage over 24 h was not different between genotypes (WT N = 10, TG N = 8). White bar on the xaxis indicates lights on and the black bar lights off.

(B) TG mice showed high exploration on both days of an open field test (WT N = 7, TG N = 9).

(C) Exploration of closed arms in the elevated plus maze did not differ between genotypes (WT N = 7, TG N = 8), indicating no change in anxiety.

(D) Active avoidance performance of the TG mice was poor compared to the control mice as they displayed a reduced proportion of successful avoidance responses at the end of the training (WT N = 7, TG N = 7).

(E) WT (N = 14) and TG mice (N = 9) showed no preference for either side of the three-compartment test system during habituation and both similarly preferred the side with a mouse during the testing of social affiliation behavior. However, social memory in a three-compartment test was impaired in TG mice, which did not display any preference for the novel interaction mouse.

(F) In a water cross maze task, the average latency of finding the platform decreased over time during the training and reversal learning, yet TG mice exhibited higher latencies during reversal (WT N = 10, TG N = 8). Values are mean ± SEM.; *$p < 0.05$ between TG and WT; $^{###}p < 0.001$ compared to chance level.

session (Student's t-test: $t(21) = 0.2204$, $p = 0.8277$). During the final test session, with the meanwhile familiarized and a novel interaction mouse (Student's t-test: $t(21) = 1.849$, $p = 0.0786$), WT mice preferred the novel interaction partner (Student's one sample ttest: $t(13) = 4.655$, $p = 0.0005$), however, TG mice failed to show a preference for the stranger (Student's one sample ttest $t(8) = 0.5991$, $p = 0.5657$), indicating impaired social memory (Figure 5E). Finally, spatial learning and reversal learning were tested using the water cross maze task. No effect of genotype on the latency for finding the platform was seen during the initial learning phase (repeated measures two-wayANOVA: training: $F(1,16) = 1.401$, $p = 0.2539$), but TG mice showed a significantly increased latency to find the platform during reversal ($F(1,6) = 7.776$, $p = 0.0316$) (Figure 5F). At the same time the number of errors was not affected by genotype during either learning or reversal learning (repeated measures two-wayANOVA: training: $F(1,16) = 1.557$, $p = 0.2301$, reversal learning: $F(1,6) = 0.179$, $p = 0.6870$). Overall, TG mice showed increased exploratory behavior and impairment in both MF-dependent learning and social memory.

DISCUSSION

In the present study, we provide evidence for a role of Ndr2 in hippocampal circuit function and connectivity *in vivo*. We demonstrate that the overexpression of Ndr2 in postmigratory forebrain neurons decreases ventral hippocampal mossy fiber fields and reduces transmission at mossy fiber terminals, resulting in altered hippocampal network activity and behavioral impairments. The human *NDR2* gene is located in a hotspot for microduplication on chromosome 12p associated with intellectual disabilities, autism and seizures. In fact, copy number variations have received increasing attention in recent years as cause for such brain dysfunction as well as general developmental delay (Girirajan et al., 2013). While we did not observe any indication of seizures or enhanced epileptiform activity in our experiments, our data clearly demonstrate that a moderate increase of Ndr2 expression in the postnatal brain is sufficient to induce significant disturbance of cognitive functions.

To address the effects of enhanced Ndr2 expression in the brain, we generated transgenic mice that conditionally express an EGFP:Ndr2 fusion protein. A major objective in our current study was to mimic the rather late postnatal increase of endogenous Ndr2 expression in the mouse brain and to enhance the expression in principle neurons of hippocampus and neocortex. For this reason, we employed a widely-used mouse line expressing Cre recombinase under the CaMKII-alpha promoter that drives expression in forebrain neurons from around P20, but not during early postnatal development (Minichiello et al., 1999). In the adult brain, as expected, we observed the transgene expression in a forebrain-specific manner and dominantly in the hippocampus MF using the EGFP tag in the transgene. The size shift of the transgenic EGFP:Ndr2 allowed us to confirm that endogenously expressed Ndr2 was quantitatively comparable between WT and TG mice and total Ndr2 (endogenous Ndr2 plus transgenic EGFP:Ndr2) protein levels were increased 90–100% in CA3 and DG, albeit only 20% in the CA1 of TG mice compared to WT. Based on the expression profile of transgenic Ndr2 we decided to focus our investigation on its effects on structure and function of the hippocampal mossy fiber system, as CaMKII-alpha driven transgene induction during late postnatal development (Minichiello et al., 1999) would likely interfere with the maturation and adult function but likely not the initial formation of the mossy fiber system (Gaarskjaer, 1985).

Expression analysis in WT mice confirmed that alongside Ndr2, various other components of the Hippo signaling pathway are endogenously expressed in granule cells of the dentate gyrus and differentially regulated during mossy fiber maturation (Figure S2). Three ages were selected for this analysis–P15, P30, and 3 months of age–to scrutinize the postnatal developmental expression profile of this pathway. Quantitative PCR results revealed a postnatal regulation of the expression of Ndr2 both in the suprapyramidal and infrapyramidal blades of the granule cell layer. Specifically, in the suprapyramidal blade, the Ndr2 mRNA levels significantly dropped at P30 and increased to a much higher level in adulthood when compared to P15. Thus, the transgene expression starts when the Ndr2 levels endogenously begin to decrease, keeping the expression higher than normal levels until and throughout adulthood. Since the mossy fiber development is mostly completed by P15 (Gaarskjaer, 1985), the Ndr2 overexpression in TG mice bypasses most granular cells completing their distal axonal projections. Interestingly, the two potential direct activators of Ndr2, Mst2 and Mst3 showed comparable regulation dynamics indicating that Hippo pathway functions may be more generally important for the postnatal development and maturation of the mossy fiber system. Furthermore, our data reveal a reduction in the number of doublecortin-positive profiles in the ventral DG in the absence of a change in Ki67 labeling, suggesting a deficit in the maturation of adult-born granule cells, but not in their rate of proliferation. It has previously been shown that CaMKII is expressed in doublecortin positive adult-born granule cells and critically involved in their maturation (Arruda-Carvalho et al., 2014). Therefore cell-intrinsic mechanisms in adult-born granule cells may well have been altered by the transgene expression. The proteomic analysis of the Ndr2 associated proteins in TG mice further suggests a modulation of RNA processing and cytoskeleton organization by the transgenic Ndr2, including actin, tubulin, and intermediate filament components (see Tables S2 and S3). We have previously reported an interaction of Ndr2 with the actin cytoskeleton in outgrowing neurites (Stork et al., 2004) and actin organization changes have been demonstrated during MF development and the activity-dependent modulation of MF terminals (Knöll et al., 2006; Owe et al., 2009; Zhang et al., 2014; Zhao et al., 2012). However, the transgenic effect appears to be independent of Ndr2 regulating beta1-integrin dependent neurite outgrowth (Rehberg et al., 2014), in line with the fact that in developing MF fascicles, beta1-integrins are not expressed (Schuster et al., 2001).

Of note, five putative direct interaction factors of Ndr2 could be identified that have previously been implicated in mossy fiber growth and plasticity: the mammalian target of rapamycin (mTOR) and c-Jun kinase

(JNK2), homologs which have been shown to interact with the Ndr2 homolog trc in the fruit fly during dendritic growth control (He et al., 2005; Koike et al., 2008), may promote the sprouting of MF in experimentally induced epilepsy (Zeng et al., 2009; Zhang et al., 2018). Protein kinase A and Syntaxin 1, homologs of which interact with the Ndr2 homolog in yeast (Ho et al., 2002; Yan et al., 2008), are involved for the expression of long-term potentiation in MF in mice (Helme-Guizon et al., 1998; Huang et al., 1995) and Lrrk2, which also interacts with Ndr2 homologs in yeast (Gupta et al., 2013) is critical for the postnatal development of DG granule cells including the expression of doublecortin (Paus et al., 2013). Our data thus indicate that the overexpression of Ndr2 in TG mice may be able to modify several intracellular signaling pathways in the adult brain that are relevant to mossy fiber growth and function. Our analysis further suggests that transgenic Ndr2, in addition to Mst2 and Mst3, may be activated by Mob2 (Couzens et al., 2013) and/or Fry (He et al., 2005). Together, these data suggest that modulation of signaling events controlling gene expression and cytoskeleton dynamics by Ndr2 and potentially other components of the Hippo pathway (Sakuma et al., 2016) alters MF growth in adult born granule cells and MF function in the mature brain. Whether these molecular interaction partners of Ndr2 may provide entry points for the development of novel intervention strategies to combat neurodevelopmental disorders, intellectual disabilities, or autism needs to be determined in future studies.

Beyond the potential cellular mechanisms of these circuitry changes, we asked whether key hippocampal functions in the generation of network activities and control of behavior may be impaired as the result of Ndr2 overexpression. Accumulating evidence suggests that MF input is critical for maintenance and modulation of network oscillations generated within the CA3 associative network, both *in vitro* and *in vivo*. Specifically, both frequency and amplitude of SW-R originating in CA3 are dependent on constitutive transmitter release from MF (Rex et al., 2009), which is in good agreement with our observation of a significantly reduced size of SW in the CA3 subregion in TG mice. Furthermore, our data match a study that provides evidence for the necessity of DG network activity in coordination of CA3 neuronal activity for both SW-R and beta/low gamma oscillations (20–50 Hz) (Sasaki et al., 2018).

As these network activity patterns have been implicated in cognitive and emotional information processing (Çalışkan and Stork, 2018), we further undertook a comprehensive behavioral analysis of the mutant mice. Mossy fiber density has previously been negatively correlated with exploratory activity in the open field (Crusio et al., 1989) and active avoidance learning (Schwegler et al., 1981), however, those studies focused primarily on the size of the infra-/intrapyramidal band. A relation between the length of the infrapyramidal band and reversal learning in the Morris water maze has also been shown previously (McNamara et al., 1998), while increased MF transmission in DG-specific GluN1 null mutants as well as hyperactivation of the ventral CA3 but not dorsal CA3 with DREADD receptors are accompanied by a disturbance of social memory (Segev et al., 2018). Our current data suggest that deficits in the suprapyramidal band of TG mice are indeed associated with altered exploratory activity and reduced performance in avoidance, social and spatial reversal learning. These effects may involve the altered network activity patterns generated in the TG mice as their decreased capacity for generation of SWs and associated ripples in the hippocampus might result in poor memory consolidation (Buzsáki, 2015; Çalışkan et al., 2016; Wilson and McNaughton, 1994). Moreover, the observed reduction in the gamma oscillations in the CA1 of the TG mice might relate to their higher exploration activity since spatial location memory has been correlated with gamma oscillations (Lu et al., 2011) and dynamic coupling and increased coherence of gamma oscillations in the CA3 and CA1 subregions appear during a spatial working memory task (Montgomery and Buzsáki, 2007). We argue that suboptimal network activity in TG mice could reduce cognitive capacity, stimulate exploration, and delay processing in a spatial reversal task. Of note, transgenic Ndr2 expression is also evident in the cortex of TG mice, which might contribute to the behavioral deficits observed in this study. Future *in vivo* studies assessing distinct network activities, e.g., theta and gamma oscillations, in cortical and hippocampal regions during corresponding behavioral tasks and their relation to regional Ndr2 expression might help overcoming this limitation.

Our findings provide new insights into the consequence of Ndr2 gene amplification and thus may be of relevance for understanding mechanisms involved in the development of intellectual disabilities in individuals with microduplications in the corresponding region of chromosome 12p11. They are also of potential relevance for the intellectual disability phenotype of the PKS. The genetic nature of the disorders leads to great individual variability and hampers the analysis of mechanisms underlying the intellectual disabilities in PKS patients. Various structural abnormalities have been reported in PKS patients, including ventricular

changes, cortical atrophy, or corpus callosum dysgenesis (Poulton et al., 2018), that are not apparent in TG mice. This discrepancy may result from the involvement of additional genes and/or the comparatively late onset of the expression of the transgene. Moreover, epilepsy is found in about one-half of PKS patients, but no seizure-like activity was observed in TG animals. However, medicated and seizure-free PKS individuals still show abnormal interictal EEG patterns (Giordano et al., 2012). The clinical picture of 12p11 microduplications is similarly diverse with several individuals showing intellectual disabilities or autism, seizures, and microcephaly (Table S1). Multiplication of the human *NDR2* gene may contribute to altered network activity and the intellectual and social phenotype in these genetic conditions.

Limitations of the study

In our current study, we developed a transgenic mouse aiming at clarifying the putative contribution of Ndr2 amplification to intellectual disability and autism induced by microduplications of NDR2. However, our mouse model does not exactly recapitulate the copy number variations present in the human population. First, relevant microduplications in humans contain at least three additional genes, which are not addressed in this paper. Second, while we have attempted to mimic the increased expression pattern of Ndr2 in late postnatal development and adulthood, changes during earlier development are not addressed with our genetic design. And finally, our phenotypic characterization is focused on the hippocampus and hippocampus-dependent behavior. A more detailed assessment of, e.g., dorsal and ventral hippocampal circuits or contribution of neocortical areas showing Ndr2 overexpression, as well as *in vivo* electrophysiological readouts will be required for a more complete picture of Ndr2-related behavioral and network activity dysfunction.

STAR★METHODS

Detailed methods are provided in the online version of this paper and include the following:

- KEY RESOURCES TABLE
- RESOURCE AVAILABILITY
  - Lead contact
  - Materials availability
  - Data and code availability
- EXPERIMENTAL MODEL AND SUBJECT DETAILS
- METHOD DETAILS
  - Animal husbandry
  - Genetic characterization of Ndr2-overexpressing transgenic mouse
  - Histological staining
  - Western blotting
  - Proteomics analysis
  - mRNA expression analysis
  - Electrophysiology
  - Sharp wave-ripples (SW-R) and gamma oscillation recordings
  - Behavioral analysis
- QUANTIFICATION AND STATISTICAL ANALYSIS

SUPPLEMENTAL INFORMATION

Supplemental information can be found online at https://doi.org/10.1016/j.isci.2021.102868.

ACKNOWLEDGMENTS

We thank A. Bohnstedt for excellent animal care, as well as S. Stork, F. Webers, and A. Koffi-von-Hoff for expert technical assistance. This study makes use of data generated by the DECIPHER community. A full list of centers who contributed to the generation of the data is available from http://decipher.sanger.ac.uk and via email from decipher@sanger.ac.uk. Funding for the DECIPHER project was provided by the Wellcome Trust. This study was supported by DFG (CRC779 to OS, MRK and TK, 362321501/RTG 2413 SynAGE to OS, MRK and AD, STO448/4-1 to OS, DI 702/8-1 to AD) and the Leibniz Association Project SAW Neurotranslation to MRK. Further support was obtained by the Center for Behavioral Brain Sciences - CBBS promoted by Europäische Fonds für regionale Entwicklung - EFRE (ZS/2016/04/78113) to GC and CBBS - Science Campus funded by the Leibniz Association (SAS-2015-LIN-LWC) to GC and OS.

AUTHOR CONTRIBUTIONS

Conceptualization, OS, KR, DAM; Methodology, OS, KR, DAM, IM, IS, TK; Investigation, DAM, GÇ, PY, KR, YED, EK, AE, HH, JRBA; Writing – Original Draft, DAM, KR, OS; Writing – Reviewing & Editing, GÇ, MRK, AD, OS; Visualization, DAM, GÇ; Funding Acquisition, OS, GÇ, AD, TK, MRK.

DECLARATION OF INTERESTS

The authors declare no competing interests.

Received: January 25, 2021
Revised: May 19, 2021
Accepted: July 14, 2021
Published: August 20, 2021

REFERENCES

Albrecht, A., Caliskan, G., Oitzl, M.S., Heinemann, U., and Stork, O. (2013a). Long-lasting increase of corticosterone after fear memory reactivation: anxiolytic effects and network activity modulation in the ventral hippocampus. Neuropsychopharmacology *38*, 386–394. https://doi.org/10.1038/npp.2012.192.

Albrecht, A., and Stork, O. (2012). Are NCAM deficient mice an animal model for schizophrenia? Front. Behav.Neurosci. *6*, 43. https://doi.org/10.3389/fnbeh.2012.00043.

Albrecht, A., Thiere, M., Bergado-Acosta, J.R., Poranzke, J., Muller, B., and Stork, O. (2013b). Circadian modulation of anxiety: a role for somatostatin in the amygdala. PLoS One *8*, e84668. https://doi.org/10.1371/journal.pone.0084668.

Andres-Alonso, M., Ammar, M.R., Butnaru, I., Gomes, G.M., Acuña Sanhueza, G., Raman, R., Yuanxiang, P., Borgmeyer, M., Lopez-Rojas, J., Raza, S.A., et al. (2019). SIPA1L2 controls trafficking and local signaling of TrkB-containing amphisomes at presynaptic terminals. Nat. Commun. *10*, 5448. https://doi.org/10.1038/s41467-019-13224-z.

Arruda-Carvalho, M., Restivo, L., Guskjolen, A., Epp, J.R., Elgersma, Y., Josselyn, S.A., and Frankland, P.W. (2014). Conditional deletion of -CaMKII impairs integration of adult-generated granule cells into dentate gyrus circuits and hippocampus-dependent learning. J. Neurosci. *34*, 11919–11928. https://doi.org/10.1523/JNEUROSCI.0652-14.2014.

Ashburner, M., Ball, C.A., Blake, J.A., Botstein, D., Butler, H., Cherry, J.M., Davis, A.P., Dolinski, K., Dwight, S.S., Eppig, J.T., et al. (2000). Gene Ontology: tool for the unification of biology. Nat. Genet. *25*, 25–29. https://doi.org/10.1038/75556.

Berger, S., Wolfer, D.P., Selbach, O., Alter, H., Erdmann, G., Reichardt, H.M., Chepkova, A.N., Welzl, H., Haas, H.L., Lipp, H.-P., and Schütz, G. (2006). Loss of the limbic mineralocorticoid receptor impairs behavioral plasticity. Proc. Natl. Acad. Sci. U S A *103*, 195–200. https://doi.org/10.1073/pnas.0503878102.

Buzsáki, G. (2015). Hippocampal sharp wave-ripple: a cognitive biomarker for episodic memory and planning. Hippocampus *25*, 1073–1188. https://doi.org/10.1002/hipo.22488.

Çalışkan, G., Albrecht, A., Hollnagel, J.O., Rösler, A., Richter-Levin, G., Heinemann, U., and Stork, O. (2015a). Long-term changes in the CA3 associative network of fear-conditioned mice. Stress *18*, 188–197. https://doi.org/10.3109/10253890.2015.1004628.

Çalışkan, G., Schulz, S.B., Gruber, D., Behr, J., Heinemann, U., and Gerevich, Z. (2015b). Corticosterone and corticotropin-releasing factor acutely facilitate gamma oscillations in the hippocampus in vitro. Eur. J. Neurosci. *41*, 31–44. https://doi.org/10.1111/ejn.12750.

Çalışkan, G., Müller, I., Semtner, M., Winkelmann, A., Raza, A.S., Hollnagel, J.O., Rösler, A., Heinemann, U., Stork, O., and Meier, J.C. (2016). Identification of parvalbumin interneurons as cellular substrate of fear memory persistence. Cereb.Cortex *26*, 2325–2340. https://doi.org/10.1093/cercor/bhw001.

Çalışkan, G., and Stork, O. (2018). Hippocampal network oscillations as mediators of behavioural metaplasticity: insights from emotional learning. Neurobiol. Learn. Mem. *154*, 37–53. https://doi.org/10.1016/j.nlm.2018.02.022.

Çalışkan, G., and Stork, O. (2019). Hippocampal network oscillations at the interplay between innate anxiety and learned fear. Psychopharmacology *236*, 321–338. https://doi.org/10.1007/s00213-018-5109-z.

Carmona-Saez, P., Chagoyen, M., Tirado, F., Carazo, J.M., and Pascual-Montano, A. (2007). GENECODIS: a web-based tool for finding significant concurrent annotations in gene lists. Genome Biol. *8*, R3. https://doi.org/10.1186/gb-2007-8-1-r3.

Chan, C., Weeber, E.J., Zong, L., Fuchs, E., Sweatt, J.D., and Davis, R.L. (2006). Beta 1-integrins are required for hippocampal AMPA receptor-dependent synaptic transmission, synaptic plasticity, and working memory. J. Neurosci. *26*, 223–232. https://doi.org/10.1523/JNEUROSCI.4110-05.2006.

Couzens, A.L., Knight, J.D.R., Kean, M.J., Teo, G., Weiss, A., Dunham, W.H., Lin, Z.-Y., Bagshaw, R.D., Sicheri, F., Pawson, T., et al. (2013). Protein interaction network of the mammalian Hippo pathway reveals mechanisms of kinase-phosphatase interactions. Sci. Signal. *6*, rs15. https://doi.org/10.1126/scisignal.2004712.

Crusio, W.E., Schwegler, H., and van Abeelen, J.H.F. (1989). Behavioral responses to novelty and structural variation of the hippocampus in mice. II. Multivariate genetic analysis. Behav. Brain Res. *32*, 81–88. https://doi.org/10.1016/S0166-4328(89)80075-0.

Demiray, Y.E., Rehberg, K., Kliche, S., and Stork, O. (2018). Ndr2 kinase controls neurite outgrowth and dendritic branching through α1 integrin expression. Front. Mol. Neurosci. *11*, 66. https://doi.org/10.3389/fnmol.2018.00066.

Dumas, T.C., Powers, E.C., Tarapore, P.E., and Sapolsky, R.M. (2004). Overexpression of calbindin D(28k) in dentate gyrus granule cells alters mossy fiber presynaptic function and impairs hippocampal-dependent memory. Hippocampus *14*, 701–709. https://doi.org/10.1002/hipo.10210.

Emoto, K. (2011). The growing role of the Hippo–NDR kinase signalling in neuronal development and disease. J. Biochem. *150*, 133–141. https://doi.org/10.1093/jb/mvr080.

Emoto, K., He, Y., Ye, B., Grueber, W.B., Adler, P.N., Jan, L.Y., and Jan, Y.-N. (2004). Control of dendritic branching and tiling by the Tricornered-kinase/Furry signaling pathway in Drosophila sensory neurons. Cell *119*, 245–256. https://doi.org/10.1016/j.cell.2004.09.036.

Evers, M.R., Salmen, B., Bukalo, O., Rollenhagen, A., Bösl, M.R., Morellini, F., Bartsch, U., Dityatev, A., and Schachner, M. (2002). Impairment of L-type Ca2+ channel-dependent forms of hippocampal synaptic plasticity in mice deficient in the extracellular matrix glycoprotein tenascin-C. J. Neurosci. *22*, 7177–7194, 20026735.

Firth, H.V., Richards, S.M., Bevan, A.P., Clayton, S., Corpas, M., Rajan, D., Van Vooren, S., Moreau, Y., Pettett, R.M., and Carter, N.P. (2009). DECIPHER: database of chromosomal imbalance and phenotype in humans using ensembl resources. Am. J. Hum. Genet. *84*, 524–533. https://doi.org/10.1016/j.ajhg.2009.03.010.

Gaarskjaer, F.B. (1985). The development of the dentate area and the hippocampal mossy fiber projection of the rat. J. Comp. Neurol. *241*, 154–170. https://doi.org/10.1002/cne.902410204.

Gallegos, M.E., and Bargmann, C.I. (2004). Mechanosensory neurite termination and tiling depend on SAX-2 and the SAX-1 kinase. Neuron

44, 239–249. https://doi.org/10.1016/j.neuron.2004.09.021.

Giordano, L., Viri, M., Borgatti, R., Lodi, M., Accorsi, P., Faravelli, F., Ferretti, M.C., Grasso, R., Memo, L., Prola, S., et al. (2012). Seizures and EEG patterns in Pallister-Killian syndrome: 13 New Italian patients. Eur. J. Paediatr. Neurol. *16*, 636–641. https://doi.org/10.1016/j.ejpn.2012.03.003.

Girirajan, S., Dennis, M.Y., Baker, C., Malig, M., Coe, B.P., Campbell, C.D., Mark, K., Vu, T.H., Alkan, C., Cheng, Z., et al. (2013). Refinement and discovery of new hotspots of copy-number variation associated with autism spectrum disorder. Am. J. Hum. Genet. *92*, 221–237. https://doi.org/10.1016/j.ajhg.2012.12.016.

Gupta, S., Mana-Capelli, S., McLean, J.R., Chen, C.-T., Ray, S., Gould, K.L., and McCollum, D. (2013). Identification of SIN pathway targets reveals mechanisms of crosstalk between NDR kinase pathways. Curr. Biol. *23*, 333–338. https://doi.org/10.1016/j.cub.2013.01.014.

Hayani, H., Song, I., and Dityatev, A. (2018). Increased excitability and reduced excitatory synaptic input into fast-spiking CA2 interneurons after enzymatic attenuation of extracellular matrix. Front. Cell.Neurosci. *12*, 149. https://doi.org/10.3389/fncel.2018.00149.

He, Y., Fang, X., Emoto, K., Jan, Y.-N., and Adler, P.N. (2005). The tricornered Ser/Thr protein kinase is regulated by phosphorylation and interacts with furry during Drosophila wing hair development. Mol. Biol. Cell *16*, 689–700. https://doi.org/10.1091/mbc.e04-09-0828.

Helme-Guizon, A., Davis, S., Israel, M., Lesbats, B., Mallet, J., Laroche, S., and Hicks, A. (1998). Increase in syntaxin 1B and glutamate release in mossy fibre terminals following induction of LTP in the dentate gyrus: a candidate molecular mechanism underlying transsynaptic plasticity. Eur. J. Neurosci. *10*, 2231–2237. https://doi.org/10.1046/j.1460-9568.1998.00232.x.

Hiroi, N., and Yamauchi, T. (2019). Modeling and predicting developmental trajectories of neuropsychiatric dimensions associated with copy number variations. Int. J. Neuropsychopharmacol. *22*, 488–500. https://doi.org/10.1093/ijnp/pyz026.

Ho, Y., Gruhler, A., Heilbut, A., Bader, G.D., Moore, L., Adams, S.-L., Millar, A., Taylor, P., Bennett, K., Boutilier, K., et al. (2002). Systematic identification of protein complexes in Saccharomyces cerevisiae by mass spectrometry. Nature *415*, 180–183. https://doi.org/10.1038/415180a.

Huang, Y.-Y., Kandel, E.R., Varshavsky, L., Brandont, E.P., Qi, M., Idzerda, R.L., Stanley McKnight, G., and Bourtchouladz, R. (1995). A genetic test of the effects of mutations in PKA on mossy fiber ltp and its relation to spatial and contextual learning. Cell *83*, 1211–1222. https://doi.org/10.1016/0092-8674(95)90146-9.

Kleinknecht, K.R., Bedenk, B.T., Kaltwasser, S.F., Grünecker, B., Yen, Y.-C., Czisch, M., and Wotjak, C.T. (2012). Hippocampus-dependent place learning enables spatial flexibility in C57BL6/N mice. Front. Behav.Neurosci. *6*, 87. https://doi.org/10.3389/fnbeh.2012.00087.

Knöll, B., Kretz, O., Fiedler, C., Alberti, S., Schütz, G., Frotscher, M., and Nordheim, A. (2006). Serum response factor controls neuronal circuit assembly in the hippocampus. Nat. Neurosci. *9*, 195–204. https://doi.org/10.1038/nn1627.

Koike, M., Shibata, M., Tadakoshi, M., Gotoh, K., Komatsu, M., Waguri, S., Kawahara, N., Kuida, K., Nagata, S., Kominami, E., et al. (2008). Inhibition of autophagy prevents hippocampal pyramidal neuron death after hypoxic-ischemic injury. Am. J. Pathol. *172*, 454–469. https://doi.org/10.2353/ajpath.2008.070876.

Kolodziej, A., Smalla, K.-H., Richter, S., Engler, A., Pielot, R., Dieterich, D.C., Tischmeyer, W., Naumann, M., and Kähne, T. (2016). High resolution quantitative synaptic proteome profiling of mouse brain regions after auditory discrimination learning. J. Vis. Exp. *2016*, 54992. https://doi.org/10.3791/54992.

Lu, C.B., Jefferys, J.G.R., Toescu, E.C., and Vreugdenhil, M. (2011). In vitro hippocampal gamma oscillation power as an index of in vivo CA3 gamma oscillation strength and spatial reference memory. Neurobiol. Learn. Mem. *95*, 221–230. https://doi.org/10.1016/j.nlm.2010.11.008.

Maier, N., Nimmrich, V., and Draguhn, A. (2003). Cellular and network mechanisms underlying spontaneous sharp wave-ripple complexes in mouse hippocampal slices. J. Physiol. *550*, 873–887. https://doi.org/10.1113/jphysiol.2003.044602.

McNamara, R.K., Stumpo, D.J., Morel, L.M., Lewis, M.H., Wakeland, E.K., Blackshear, P.J., and Lenox, R.H. (1998). Effect of reduced myristoylated alanine-rich C kinase substrate expression on hippocampal mossy fiber development and spatial learning in mutant mice: transgenic rescue and interactions with gene background. Proc. Natl. Acad. Sci. U S A *95*, 14517–14522. https://doi.org/10.1073/PNAS.95.24.14517.

Minichiello, L., Korte, M., Wolfer, D., Kühn, R., Unsicker, K., Cestari, V., Rossi-Arnaud, C., Lipp, H.P., Bonhoeffer, T., and Klein, R. (1999). Essential role for TrkB receptors in hippocampus-mediated learning. Neuron *24*, 401–414. https://doi.org/10.1016/S0896-6273(00)80853-3.

Montgomery, S.M., and Buzsáki, G. (2007). Gamma oscillations dynamically couple hippocampal CA3 and CA1 regions during memory task performance. Proc. Natl. Acad. Sci. U S A *104*, 14495–14500. https://doi.org/10.1073/pnas.0701826104.

Muller, I., Obata, K., Richter-Levin, G., and Stork, O. (2014). GAD65 haplodeficiency conveys resilience in animal models of stress-induced psychopathology. Front. Behav.Neurosci. *8*, 265. https://doi.org/10.3389/fnbeh.2014.00265.

Niwa, H., Yamamura, K., and Miyazaki, J. (1991). Efficient selection for high-expression transfectants with a novel eukaryotic vector. Gene *108*, 193–199. https://doi.org/10.1016/0378-1119(91)90434-d.

Owe, S.G., Jensen, V., Evergren, E., Ruiz, A., Shupliakov, O., Kullmann, D.M., Storm-Mathisen, J., Walaas, S.I., Hvalby, Ø., and Bergersen, L.H. (2009). Synapsin- and actin-dependent frequency enhancement in mouse hippocampal mossy fiber synapses. Cereb. Cortex *19*, 511–523. https://doi.org/10.1093/cercor/bhn101.

Pallister, P.D., Meisner, L.F., Elejalde, B.R., Francke, U., Herrmann, J., Spranger, J., Tiddy, W., Inhorn, S.L., and Opitz, J.M. (1977). The pallister mosaic syndrome. Birth Defects Orig. Artic. Ser. *13*, 103–110.

Papatheodoropoulos, C., and Kostopoulos, G. (2002). Spontaneous, low frequency (~2–3 Hz) field activity generated in rat ventral hippocampal slices perfused with normal medium. Brain Res. Bull. *57*, 187–193. https://doi.org/10.1016/S0361-9230(01)00738-9.

Paus, M., Kohl, Z., Ben Abdallah, N.M.B., Galter, D., Gillardon, F., and Winkler, J. (2013). Enhanced dendritogenesis and axogenesis in hippocampal neuroblasts of LRRK2 knockout mice. Brain Res. *1497*, 85–100. https://doi.org/10.1016/j.brainres.2012.12.024.

Peltomäki, P., Knuutila, S., Ritvanen, A., Kaitila, I., and Chapelle, A.D.L.A. (1987). Pallister-Killian syndrome: cytogenetic and molecular studies. Clin.Genet. *31*, 399–405. https://doi.org/10.1111/j.1399-0004.1987.tb02832.x.

Perez-Riverol, Y., Csordas, A., Bai, J., Bernal-Llinares, M., Hewapathirana, S., Kundu, D.J., Inuganti, A., Griss, J., Mayer, G., Eisenacher, M., et al. (2019). The PRIDE database and related tools and resources in 2019: improving support for quantification data. Nucleic Acids Res. *47*, D442–D450. https://doi.org/10.1093/nar/gky1106.

Poulton, C., Baynam, G., Yates, C., Alinejad-Rokny, H., Williams, S., Wright, H., Woodward, K.J., Sivamoorthy, S., Peverall, J., Shipman, P., et al. (2018). A review of structural brain abnormalities in Pallister-Killian syndrome. Mol. Genet. Genomic Med. *6*, 92–98. https://doi.org/10.1002/mgg3.351.

Rehberg, K., Bergado-Acosta, J.R., Koch, J.C., and Stork, O. (2010). Disruption of fear memory consolidation and reconsolidation by actin filament arrest in the basolateral amygdala. Neurobiol. Learn. Mem. *94*, 117–126. https://doi.org/10.1016/j.nlm.2010.04.007.

Rehberg, K., Kliche, S., Madencioglu, D.A., Thiere, M., Müller, B., Meineke, B.M., Freund, C., Budinger, E., and Stork, O. (2014). The serine/threonine kinase Ndr2 controls integrin trafficking and integrin-dependent neurite growth. J. Neurosci. *34*, 5342–5354. https://doi.org/10.1523/JNEUROSCI.2728-13.2014.

Rex, C.S., Colgin, L.L., Jia, Y., Casale, M., Yanagihara, T.K., Debenedetti, M., Gall, C.M., Kramar, E.A., and Lynch, G. (2009). Origins of an intrinsic hippocampal EEG pattern. PLoS One *4*, e7761. https://doi.org/10.1371/journal.pone.0007761.

Sakuma, C., Saito, Y., Umehara, T., Mosca, T.J., Miura, M., Chihara, T., Kamimura, K., and Maeda, N. (2016). The strip-hippo pathway regulates synaptic terminal formation by modulating actin organization at the Drosophila neuromuscular synapses. Cell Rep. *16*, 2289–2297. https://doi.org/10.1016/j.celrep.2016.07.066.

Sasaki, T., Piatti, V.C., Hwaun, E., Ahmadi, S., Lisman, J.E., Leutgeb, S., and Leutgeb, J.K. (2018). Dentate network activity is necessary for

spatial working memory by supporting CA3 sharp-wave ripple generation and prospective firing of CA3 neurons. Nat. Neurosci. *21*, 258–269. https://doi.org/10.1038/s41593-017-0061-5.

Schildt, S., Endres, T., Lessmann, V., and Edelmann, E. (2013). Acute and chronic interference with BDNF/TrkB-signaling impair LTP selectively at mossy fiber synapses in the CA3 region of mouse hippocampus. Neuropharmacology *71*, 247–254. https://doi.org/10.1016/J.NEUROPHARM.2013.03.041.

Schinzel, A. (1991). Tetrasomy 12p (Pallister-Killian syndrome). J. Med. Genet. *28*, 122–125. https://doi.org/10.1136/jmg.28.2.122.

Schmued, L., and Slikker, W. (1999). Black-Gold: a simple, high-resolution histochemical label for normal and pathological myelin in brain tissue sections. Brain Res. *837*, 289–297. https://doi.org/10.1016/S0006-8993(99)01624-8.

Schuster, T., Krug, M., Stalder, M., Hackel, N., Gerardy-Schahn, R., and Schachner, M. (2001). Immunoelectron microscopic localization of the neural recognition molecules L1, NCAM, and its isoform NCAM180, the NCAM-associated polysialic acid, beta1 integrin and the extracellular matrix molecule tenascin-R in synapses of the adult rat hippocampus. J. Neurobiol. *49*, 142–158. https://doi.org/10.1002/neu.1071.

Schwegler, H., Lipp, H.P., Van der Loos, H., and Buselmaier, W. (1981). Individual hippocampal mossy fiber distribution in mice correlates with two-way avoidance performance. Science *214*, 817–819. https://doi.org/10.1126/science.7292015.

Segev, A., Yanagi, M., Scott, D., Southcott, S.A., Lister, J.M., Tan, C., Li, W., Birnbaum, S.G., Kourrich, S., and Tamminga, C.A. (2018). Reduced GluN1 in mouse dentate gyrus is associated with CA3 hyperactivity and psychosis-like behaviors. Mol. Psychiatry *25*, 2832–2843. https://doi.org/10.1038/s41380-018-0124-3.

Stork, O., Zhdanov, A., Kudersky, A., Yoshikawa, T., Obata, K., and Pape, H.-C. (2004). Neuronal functions of the novel serine/threonine kinase Ndr2. J. Biol. Chem. *279*, 45773–45781. https://doi.org/10.1074/jbc.M403552200.

Tabas-Madrid, D., Nogales-Cadenas, R., and Pascual-Montano, A. (2012). GeneCodis3: a non-redundant and modular enrichment analysis tool for functional genomics. Nucleic Acids Res. *40*, W478–W483. https://doi.org/10.1093/nar/gks402.

Teschler-Nicola, M., and Killian, W. (1981). Case report 72: mental retardation, unusual facial appearance, abnormal hair. Synd Ident *7*, 6–7.

Ultanir, S.K., Hertz, N.T., Li, G., Ge, W.-P., Burlingame, A.L., Pleasure, S.J., Shokat, K.M., Jan, L.Y., and Jan, Y.-N. (2012). Chemical genetic identification of NDR1/2 kinase substrates AAK1 and Rabin8 Uncovers their roles in dendrite arborization and spine development. Neuron *73*, 1127–1142. https://doi.org/10.1016/j.neuron.2012.01.019.

Vandecasteele, M., Varga, V., Berényi, A., Papp, E., Barthó, P., Venance, L., Freund, T.F., and Buzsáki, G. (2014). Optogenetic activation of septal cholinergic neurons suppresses sharp wave ripples and enhances theta oscillations in the hippocampus. Proc. Natl. Acad. Sci. U S A *111*, 13535–13540. https://doi.org/10.1073/pnas.1411233111.

von Mering, C., Jensen, L.J., Snel, B., Hooper, S.D., Krupp, M., Foglierini, M., Jouffre, N., Huynen, M.A., and Bork, P. (2005). STRING: known and predicted protein-protein associations, integrated and transferred across organisms. Nucleic Acids Res. *33*, D433–D437. https://doi.org/10.1093/nar/gki005.

Wilson, M.A., and McNaughton, B.L. (1994). Reactivation of hippocampal ensemble memories during sleep. Science *265*, 676–679. https://doi.org/10.1126/science.8036517.

Yan, H., Ge, W., Chew, T.G., Chow, J.Y., McCollum, D., Neiman, A.M., and Balasubramanian, M.K. (2008). The meiosis-specific sid2p-related protein Slk1p regulates forespore membrane assembly in fission yeast. Mol. Biol. Cell *19*, 3676–3690. https://doi.org/10.1091/mbc.e07-10-1060.

Zemankovics, R., Veres, J.M., Oren, I., and Hájos, N. (2013). Feedforward inhibition underlies the propagation of cholinergically induced gamma oscillations from hippocampal CA3 to CA1. J. Neurosci. *33*, 12337–12351. https://doi.org/10.1523/JNEUROSCI.3680-12.2013.

Zeng, L.-H., Rensing, N.R., and Wong, M. (2009). The mammalian target of rapamycin signaling pathway mediates epileptogenesis in a model of temporal lobe epilepsy. J. Neurosci. *29*, 6964–6972. https://doi.org/10.1523/JNEUROSCI.0066-09.2009.

Zhang, W., Wang, X., Yu, M., Li, J.-A., and Meng, H. (2018). The c-Jun N-terminal kinase signaling pathway in epilepsy: activation, regulation, and therapeutics. J. Recept. Signal.Transduct. Res. *38*, 492–498. https://doi.org/10.1080/10799893.2019.1590410.

Zhang, Y.-F., Li, S.-L., Xiong, T.-Q., Yang, L.-B., Li, Y.-N., Tan, B.-H., Liu, Q., and li, Y.-C. (2014). The rearrangement of filamentous actin in mossy fiber synapses in pentylenetetrazol-kindled C57BL/6 mice. Epilepsy Res. *108*, 20–28. https://doi.org/10.1016/J.EPLEPSYRES.2013.10.019.

Zhao, S., Studer, D., Chai, X., Graber, W., Brose, N., Nestel, S., Young, C., Rodriguez, E.P., Saetzler, K., and Frotscher, M. (2012). Structural plasticity of spines at giant mossy fiber synapses. Front. Neural Circuits *6*, 103. https://doi.org/10.3389/fncir.2012.00103.

STAR★METHODS

KEY RESOURCES TABLE

REAGENT or RESOURCE	SOURCE	IDENTIFIER
Antibodies		
Rabbit anti-doublecortin antibody	Abcam	Cat# ab18723; RRID:AB_732011
Rabbit anti-GAPDH antibody	Cell Signaling Technologies	Cat# 5174; RRID:AB_10622025
Goat anti-GFP antibody	Abcam	Cat# ab6673; RRID:AB_305643
Rabbit anti-Ki67 antibody	Abcam	Cat# ab15580; RRID:AB_443209
Rabbit anti-Ndr2 antibody	Stork et al. (2004)	https://doi.org/10.1074/jbc.m403552200
Mouse anti-Ndr2 antibody	OriGene	Cat# TA505176; RRID:AB_2622897
Chemicals, peptides, and recombinant proteins		
Myelin stain Black-Gold II	Histo-Chem Inc.	http://www.histo-chem.com/Products.html
NMDA receptor antagonist D-AP5	Tocris	Cat. No. 0106
mGluR receptor agonist (2S, 2'R, 3'R)-2-(2', 3'dicarboxycyclopropyl) glycine (DCG-IV)	Tocris	Cat. No. 0975
Acetylcholinreceptor agonist Carbachol	Tocris	Cat. No. 2810
Critical commercial assays		
Immunostaining Vectastain Elite ABC Kit	Vector Laboratories Inc.	Cat. No. PK-6100
Protein concentration Bradford assay	Bio-Rad Laboratories Inc.	Cat. No. 5000201
µMACS GFP Cell Isolation kit	Miltenyi Biotec	Cat. No. 130-091-125
RNeasy plus micro kit for RNA isolation from tissue	Qiagen	Cat. No. 74034
Sensiscript RT kit for reverse transcription	Qiagen	Cat. No. 205213
TaqMan™ copy number reference assay, mouse,	Thermo Fisher Scientific	Cat. No. 4458366
Deposited data		
Mass spectrometry proteomics	This paper	ProteomeXchange: PXD026867
Experimental models: Organisms/strains		
Mouse: C57BL/6 wild type	M&B Taconic	B6JBOM
Mouse: Camk2a-Cre driver	Artemis Pharmaceuticals	Tg(Camk2a-cre)159Kln
Mouse: conditional Ndr2 transgenic line 55	This paper	Tg(CAG-Egfp::Stk38l)55Stork
Mouse: conditional Ndr2 transgenic line 89	This paper	Tg(CAG-Egfp::Stk38l)89Stork
Oligonucleotides		
See Table S5		
Recombinant DNA		
Transgene backbone: pCAGGS plasmid	Niwa et al. (1991)	RIKEN BRC, RRC ID RDB08938
Software and algorithms		
Mass-spec data analysis: PEAKS Studio 8.0	Bioinformatics Solutions Inc.	https://www.bioinfor.com/peaks-studio/
Video tracking software AnyMaze	Stoelting Co.	https://www.stoeltingco.com/anymaze.html
Data analysis software Prism	GraphPad Software, Inc.	https://www.graphpad.com/scientific-software/prism/
Data analysis software SigmaPlot	Systat Software Inc.	http://www.sigmaplot.co.uk/products/sigmaplot/sigmaplot-details.php
Proteome analysis: Genecodis	Tabas-Madrid et al. (2012)	https://doi.org/10.1093/nar/gks402

(*Continued on next page*)

Continued

REAGENT or RESOURCE	SOURCE	IDENTIFIER
Proteome analysis: Gene Ontology	Ashburner et al. (2000)	https://doi.org/10.1038/75556
Electrophysiology data analysis: MATLAB	MathWorks	https://www.mathworks.com
Electrophysiology data analysis: MATLAB algorithms	Çalışkan et al., 2015b	https://doi.org/10.3109/10253890.2015.1004628
Electrophysiology data analysis: Spike2 (version 8)	Cambridge Electronic Design	http://ced.co.uk/products/spkovin

RESOURCE AVAILABILITY

Lead contact

Further information and requests for resources and reagents should be directed to and will be fulfilled by the lead contact, Oliver Stork (oliver.stork@ovgu.de).

Materials availability

All unique reagents and all mouse lines generated in this study are available from the lead contact without restriction.

Data and code availability

- Proteomics data have been deposited at ProteomeXchange and are publicly available as of the date of publication. The dataset identifier / accession number is given in the key resources table.
- All data reported in this paper will be shared by the lead contact upon request.
- This study did not generate original code.
- Any additional information required to reanalyze the data reported in this paper is available from the lead contact upon request.

EXPERIMENTAL MODEL AND SUBJECT DETAILS

Ndr2 transgenic mice were generated by cloning EGFP::Ndr2 into the pCAGGS plasmid, kindly provided by Dr. K. Miyashita from Kyoto University, using restriction sites for SalI and SacII. The resulting plasmid containing the CAG and loxP sites was injected into the pronucleus of a zygote originated from CB6F2 mice by PolyGene and the transfected fertilized eggs were transferred to pseudopregnant C57BL/6 mice. CaMKIIalpha-Cre (Tg(Camk2a-cre)159Kln) mice, which are widely used to study functions of adult forebrain neurons, were used for activating the transgene expression. C57BL/6BomTac (M&B Taconic, Germany) mice were used for molecular experiments as indicated.

METHOD DETAILS

Animal husbandry

All mice were bred and maintained in the facility of Institute of Biology, Otto-von-Guericke-University Magdeburg under specific pathogen free conditions with an inverted 12-h dark/light cycle (lights off at 7 am with 30 min of dim phase), *ad libitum* food and water, group-housed 2-6 mice per cage. All experiments were conducted with experimentally naïve mice, during their active phase in the dark cycle. Male mice, 3–6-month-old, participating in the behavioral experiments were single caged one week prior to the experiments. A potential effect of animal sex on behavior, brain anatomy or physiology was not addressed in this study. Animal experiments and housing were in accordance with European regulations and approved by Landesverwaltungsamt Saxony-Anhalt (Permission numbers: 42502-2-862 UniMD and 42502-2-1284 UniMD).

Genetic characterization of Ndr2-overexpressing transgenic mouse

Offspring that carried the insertion was tested by PCR with primers (Table S5) amplifying a sequence fragment of the fusion protein EGFP::Ndr2: Forward: 5′-TCAAGATCCGCCACAACAT-3′: and Reverse: 5′-CG TGCACAAACCAAAATCAG-3′. Samples were initially denatured at 95°C for 5 min and run for 35 cycles

consisting of 15 s at 94°C, 30 s at 52°C, and 2 min at 72°C, and completed with a final extension stage at 72°C for 7 min. Tandem insertion was tested with polyA forward-primer (5′-ACGAGCCGGAAGCATA AAGTGTAAAG-3′) and CAG reverse-primer (5′-GGGGGAGATGGGGAGAGTGAAG-3′). The number of copies inserted into the genome was analyzed with the TaqMan™ copy number reference assay (mouse, TFRC, Thermo Fisher Scientific, Waltham, MA, USA) using heterozygous mice for the transgene. Samples ran for 40 cycles consisting of 15 s at 95°C and 60 s at 60°C, with an initial step of 10 min at 95°C. The primers used in the assay were: Forward: 5′-CTTTGATGACTTCCCTGAGTCTGAT-3′, Reverse: 5′-GGATTTGTAGT CGGGCTCTGT-3′, and reporter: 5′-ATTCGGCACTGGCTGTAAG-3′ (Table S5). Mice were backcrossed to C57Bl6/BomTac genetic background for more than 10 generations before behavioral and physiological testing.

Histological staining

Mice were anesthetized with a ketamine (80 mg/ml)-xylazine (6 mg/ml) mixture (1 mg/kg body weight) and were transcardially perfused using Tyrode buffer (for Timm's staining: sulfide buffer: in dH_2O 0.15 M Sodium sulfide, 0.1 M Disodium phosphate) followed by 4% paraformaldehyde (PFA) in Phosphate Buffered Saline (PBS; Timm's staining: 2% Phosphate/Glutaraldehyde buffer). Brains were removed, kept in 4% PFA in PBS for 24 h, in 30% Saccharose buffer in PBS for 48 h, then snap frozen and stored at -20°C. 30 μm thick coronal sections were cut with a cryostat for immunostaining and for the Black-Gold staining method.

Immunostaining of the transgenic Ndr2 was done on free-floating sections treated for 10 min with 0.3% H_2O_2, 5% methanol in 0.1 M phosphate buffer (PB). Sections were washed with PB, incubated for 2 h with 10% serum of the species that the secondary antibody was raised in and 10% BSA in PB. Primary antibody (goat anti-GFP, 1:500, Abcam, UK) incubation was done for two days at 4°C with 2% serum and 2% BSA in PB. After washing with PB, sections were incubated with the biotin-coupled secondary antibody (1:250) in 2% BSA in PB for 2 h at room temperature followed by 1 h incubation at room temperature with Avidin-Biotin-Complex (Vectastain Elite ABC Kit, Vector Laboratories Inc., Bulingame, CA, USA). Sections were washed and incubated in diaminobenzidine solution in PB (0.5 mg/ml) for 5 min. The development was stopped with PB. Sections were placed on slides and air-dried, and then covered with Entellan™ (Merck, Germany).

For doublecortin / Ki67 immunofluorescence staining, sections underwent antigen retrieval for 1h (90°C in 10mM sodium citrate buffer, ph6.0) before permeabilization for 30 min with 0.5% triton-X100 in PBS and blocking with 10% goat normal serum in 0.1% Triton-X100 in PBS for 1 h. Anti-doublecortin (Abcam, ab18723, 1:1500) was incubated over night at 4°C in 1% Triton-x100 in PBS and detected with donkey anti-rabbit secondary antibodies. Subsequently, anti-Ki67 antibody (Abcam ab15580, 1:500) was incubated in the same manner and detected with biotinylated secondary antibodies and fluorescence-labelled Streptavidin (all Abcam). Sections were washed three times in PBS between all incubation steps and mounted on slide glasses with Immunomount™ for inspection.

Black-Gold staining was done as described (Schmued and Slikker, 1999). In brief, sections were thaw-mounted onto gelatin-coated slides, and after rehydration in ddH_2O were incubated in 65°C Black-Gold solution (0.2% m/v Black-Gold II, Histo-Chem Inc., Jefferson, AR, USA) for 13 min. The reaction was stopped by washing with ddH_2O for 2 min. Staining was fixed with 1% sodium thiosulphate for 3 min, followed by 15 min washing with ddH_2O. Sections were dried at 50°C, incubated in xylene for 2 min and covered with Entellan™ (Merck, Germany).

For **Timm's staining**, after perfusion, brains were incubated in 20% glucose/ 2% glutaraldehyde solution overnight and frozen on dry ice. 40 μm thick horizontal sections were cut with a cryostat throughout the dorso-ventral extension of the hippocampus. Sections were mounted onto slides, dried on a heating plate and immersed in Timm's staining buffer (in ddH_2O 0.13 M citric acid, 0.08 M tri-sodium citrate dihydrate, 0.15 M hydroquinone, 30% gum arabic, 5 mM silver nitrate) for 30 min at 25°C. Development was stopped with dH_2O for 10 min and sections were fixed in 1% sodium thiosulfate for 5 min. After washing with dH_2O, counterstaining was done with 3% methylene blue solution (Sigma-Aldrich, Germany) for 10 s. Sections were dehydrated with 1-min steps in 70% ethanol, 95% ethanol, 100% ethanol, and xylene, and were covered with Entellan™ (Merck, Germany). For assessment of the dorsal hippocampus three sections each taken 750μm apart between Bregma – 3.8 and – 5.8 were

evaluated per animal and averaged. For the ventral hippocampus two sections per animal were considered in the range Bregma – 6.5 to -7.5.

Western blotting

Transgenic mice were bred with CaMKIIalpha-Cre +/- mice, and the expression of the transgene Ndr2 in the brain was investigated with immunoprecipitation. The forebrain of adult mice was homogenized with RIPA buffer (50 mM Tris-HCL, 150 mM NaCl, 1% Nonidet P-40, 0.5% sodium deoxycholate, 0.1% SDS, 1 mM PMSF proteinase inhibitor (Sigma-Aldricht, Germany)). The lysate was incubated for 2 h rotating at 4°C followed by centrifugation for 1 h at 16000 g at 4°C. The protein concentration of the supernatant was determined with a Bradford assay (Bio-Rad Laboratories Inc., Hercules, CA, USA). The protein samples were precleared with G-Sepharose for 1 h at 4°C, followed by centrifugation at 12000 g for 30 s. The resulting supernatant was incubated with goat anti-GFP (Abcam, UK, 1:1000) antibody rotating overnight at 4°C. Protein G-Sepharose was added and the mixture was incubated for 4 h at 4°C before precipitation of aggregates by centrifugation at 12000 g and washed with lysis buffer. The pellet was collected and incubated together with 1x loading buffer (4x: 252 mM Tris-HCl pH 6.8, 8% SDS, 40% glycerol, 0.04% bromophenol blue) for 10 min at 98°C. The samples were run on an SDS-PAGE followed by blotting onto a PVDF membrane.

Adult brain tissue was lysed on ice with lauryl maltosid lysis buffer, (1% lauryl maltoside N-dodycyl-D-maltoside, 1% NP-40, 1 mM Na_3VO_4, 2mM EDTA, 50 mM Tris-HCl, 150 mM NaCl, 0.5% DOC, 1 mM AEBSF, 1 μM pepstatin A, 1 mM NaF, 1 tablet Pierce protease inhibitor (Thermo Fisher Scientific, Waltham, MA, USA), using a tissue grinder, rotated at 4°C for 30 min then centrifuged for 30 min at 4°C at 16000 g. Protein concentration was determined using the Bradford Assay (Bio-Rad Laboratories Inc., Hercules, CA, USA) according to the manufacturer's instructions. Samples were separated on a 10% SDS-PAGE and transferred to a PVDF membrane (Immobilon-FL, Millipore, Germany). Membranes were incubated with primary antibodies mouse anti-Ndr2 (1:1000, OriGene Technologies Inc., Rockville, MD, USA) and rabbit anti-GAPDH (1:1500, Cell Signaling Technology, Danvers, MA, USA), followed by secondary antibody incubation with IRDye (1:10000, LI-COR Inc., Lincoln, NE, USA) and scanning with an Odyssey scanner (LI-COR).

Proteomics analysis

Ndr2-GFP pull down was performed using the μMACS GFP Isolation kit (Miltenyi Biotec, Germany) following the manufacturer's instructions. Captured proteins were eluted with hot Laemmli buffer and subjected to an SDS-PAGE. Each lane was divided into eight sections to perform in-gel digestion according to (Kolodziej et al., 2016). Resulting peptides were dissolved in 5 μL 0.1% trifluoroacetic acid (TFA) and purified on ZIP-TIP, C18-nanocolumns (Millipore, Billerica, MA, USA). The peptides were eluted in 7 μl of 70% (v/v) acetonitrile (ACN) and subsequently dried in a vacuum centrifuge. LC-MS/MS was performed on a hybrid dual pressure linear ion trap/orbitrap mass spectrometer (LTQ Orbitrap Velos Pro, Thermo Scientific, San Jose, CA, USA) equipped with an EASY-nLC Ultra HPLC (Thermo Scientific, San Jose, CA, USA). The peptide samples were dissolved in 10 μL of 2% ACN/0.1% TFA and fractionated on a 75 μm I.D., 25 cm PepMap C18-column, packed with 2 μm resin (Dionex, Germany). Separation was achieved by applying a gradient from 2% ACN to 35% ACN in 0.1% formic acid (FA) over a 150 min gradient at a flow rate of 300 nL/min. The LTQ Orbitrap Velos Pro MS exclusively used CID-fragmentation when acquiring MS/MS spectra, consisting of an orbitrap full MS scan followed by up to 15 LTQ MS/MS experiments (TOP15) on the most abundant ions detected in the full MS scan. The essential MS settings were as follows: full MS (FTMS; resolution 60,000; m/z range 400–2000); MS/MS (Linear Trap; minimum signal threshold 500; isolation width 2 Da; dynamic exclusion time setting 30 s; singly charged ions were excluded from selection). Normalized collision energy was set to 35%, and the activation time was set to 10 ms. Raw data processing and protein identification of the high resolution orbitrap datasets were performed with de novo sequencing algorithms of PEAKS Studio 8.0 (Bioinformatics Solutions Inc., Waterloo, Canada). The false discovery rate was set to <1%.

The obtained list of proteins was fed into a meta-analysis for the Gene Ontology (Ashburner et al., 2000) annotations of the biological processes using Genecodis (Tabas-Madrid et al., 2012). The result of the analysis was filtered for significantly enriched terms associated to the predefined parental terms "nervous system process","nervous system development " (according to the scope of this study), "protein transport","cytoskeleton organization","gene expression" and "protein phosphorylation" (according to most

prominent annotations and previously identified cellular functions of the kinase) using the term hierarchy of the Gene Ontology. Child terms of each filter term within the hierarchy were used as a lookup table to find the matching terms inside of the meta-analysis result. Evidence for potential direct interactions between Ndr2 and the resulting group of proteins was further collected using STRING, using low confidence settings to search for data from other species including yeast and a limitation to experimental data (von Mering et al., 2005). The mass spectrometry proteomics data have been deposited to the ProteomeXchange Consortium via the PRIDE (Perez-Riverol et al., 2019) partner repository with the dataset identifier PXD026867.

mRNA expression analysis

Mice were sacrificed at postnatal (P) day 15, 30, and 3 months of age by cervical dislocation. Brains were quickly removed from the skull, embedded in Tissue-Tek^{TM} OCT compound (Sakura Finetek Europe, The Netherlands) and frozen in liquid nitrogen-cooled 2-methylbutane. 20 μm-thick horizontal sections were cut on a cryostat at the level of ventral hippocampus and thaw mounted onto PLL-coated MembraneSlide 1.0 PEN slides (Zeiss, Germany). Sections were fixed in cold (-20°C) 70% ethanol, followed by a brief cresyl violet (1% m/v in 50% ethanol) staining, and dehydration for each 1min in 70% and 96% ethanol respectively. The granular cell layers of the dentate gyrus were then microdissected using a P.A.L.M. laser microbeam system (Zeiss, Germany). The collected tissues were lysed and RNA was isolated using RNeasy plus micro kit (Qiagen, Hilden, Germany) according to the manufacturer's instructions. First-strand synthesis was done with Sensiscript reverse transcriptase (QIAGEN, Germany) at 37°C for 60 min in the presence of RNase inhibitor (20 U/μl) (Thermo Fisher Scientific, Waltham, MA, USA). Quantitative real-time PCR was done with Step-One-System (Applied Biosystems, Germany) using TaqMan^{TM} reagents. The assays used were: Ndr1: Mm00506499_m1, Ndr2: Forward: 5'-TGCCCGTCTCTGAGAAGC-3', Reverse: 5'-CCACCA TTCCCAATTCTGTTTCAG-3', and reporter: 5'-ACTTGATTCTCAGATTTTG -3', Lats1: Mm01191886_m1, Lats2: Mm00497217_m1, Mst2: Mm00490480_m1, Mst3: Mm00520930_m1. VIC-labeled GAPDH assay (4352339E, Applied Biosystems, Germany) was used as a housekeeping gene. Samples were run in triplicate for 40 cycles consisting of 15 s at 95°C and 1 min at 60°C with an initial denaturation step for 10 min at 95°C and a decontamination step with uracil-N-glycosidase for 2 min at 50°C before entering the cycle.

Electrophysiology

Mossy fiber-CA3 synapse LTP (Andres-Alonso et al., 2019). Adult mice were decapitated under deep isoflurane anesthesia. Transverse slices (350 μm) from the ventral and dorsal portions of the hippocampus were cut using a vibratome (LeicaVT1000S, Nussloch, Germany) and transferred to a chamber for submerged recording conditions. Before the recording, hippocampal slices were pre-incubated for at least 1 h with carbogenated (95% O_2, 5%CO_2) artificial cerebrospinal fluid (ACSF, containing in mM: 110 NaCl, 2.5 KCl, 4 CaCl2·2H2O, 4 MgSO4·7H2O, 1.24 KH2PO4, 10 glucose, 27.4 NaHCO3, pH 7.3) at room temperature. Field excitatory postsynaptic potentials (fEPSPs) were evoked with ACSF-filled glass capillary microelectrodes (3-5 MΩ).

Identification and recordings of mossy fiber responses were performed as previously described (Evers et al., 2002). In detail, the stimulation electrode was placed in the granule cell layer of the dentate gyrus, and fEPSPs were recorded extracellularly in stratum lucidum of CA3 with stainless steel electrodes (Schildt et al., 2013). After obtaining an input-output (I-O) curve with stimulation intensities ranging from 0.5 to 6 V, stimulation intensity resulting in 15-20% of maximal fEPSP amplitude was determined and used for the rest of the stimulation protocols. Train facilitation (TF, 6 pulses at 20 Hz, repeated 3x at 0.05 Hz) and frequency facilitation (FF, 4 pulses at 0.05 Hz, and subsequently 90 pulses at 1 Hz) were tested and considered to represent mossy fiber signals when the ratio of the amplitude of the last pulse compared to the first pulse both in TF and FF exceed 200% of initial amplitudes. Before induction of mossy fiber LTP, the baseline responses were recorded with the stimuli applied every 30 s for at least 15 min. Then, MF-LTP was induced by 4 trains high-frequency stimulation (HFS) protocol (15-20% of maximum amplitude of each fEPSP according to I/O curve, at 100 Hz with 1 s duration, repeated with an interval time 20s). The NMDAR antagonist D-AP5 (50 μM, Tocris) was applied 15 min before and during HFS, and then washed out after LTP induction. The fEPSP responses were recorded for 1 h after LTP induction. At the end of every experiment, the group II metabotropic glutamate receptor agonist (2S, 2'R, 3'R)-2-(2', 3'dicarboxycyclopropyl) glycine (DCG-IV, 2μM, Tocris) was applied to confirm fEPSPs as MF signals and data were included when the inhibition was more than 70%.

Schaffer collateral-CA1 LTP. Preparation of hippocampal slices was performed as described previously (Hayani et al., 2018). Briefly, 4-month-old male mice were decapitated after fast cervical dislocation. The brain was exposed, rapidly dissected, and transferred into ice-cold ACSF containing in mM: 124 NaCl, 25 $NaHCO_3$, 17 D-glucose, 2.5 KCl, 1.24 NaH_2PO_4, 2 $CaCl_2$, and 1.5 $MgCl_2$, pH 7.4 and the osmolality was adjusted to 305 ± 5 mOsm (Chan et al., 2006). The hippocampi were dissected and 400 μm-thick transverse hippocampal slices were prepared using vibrating blade microtome (Leica VT1200S, Leica Biosystems). The slices were incubated in ACSF in an interface chamber for 2 h at room temperature for recovery. Next, the slices were transferred to the submerged recording chamber and were constantly perfused with ACSF at 30°C. ACSF was continuously saturated with 95% O_2 and 5% CO_2.

ACSF-filled glass electrodes (2-3 MΩ) were used for recording fEPSPs in CA1 stratum radiatum in response to stimulation of Schaffer collaterals. Long-term potentiation (LTP) in CA3-CA1 area was induced using high frequency stimulation (HFS) protocol of 2 trains of 100 Hz for 1 s with a 20-s interval in between, at a stimulus intensity that generated 50% of the maximum fEPSP response (Chan et al., 2006). Stimulus-response curve was recorded for a range of stimulus intensities (20 μA – 120 μA) with 10 μA increment. Paired-pulse-facilitation (PPF) was measured at five different interstimulus intervals (10, 20, 50, 100, and 200 ms). The stimulus artefacts were blanked to facilitate visual inspection of traces.

Sharp wave-ripples (SW-R) and gamma oscillation recordings

Horizontal brains slices (~400 μm) containing ventral hippocampus were cut in ice-cold, carbogenated (5% CO_2 / 95% O_2) ACSF containing (in mM) 129 NaCl, 21 NaHCO3, 3 KCl, 1.6 CaCl2, 1.8 MgCl, 1.25 NaH2PO4 and 10 glucose (pH 7.4, ~300 mOsm). Slices were transferred to an interface chamber perfused with ACSF at 32 ± 0.5°C (flow rate: 2.0 ± 0.2 ml/min). Before starting recordings, slices were incubated at least for an hour. Extracellular field recordings were obtained with glass electrodes filled with ACSF (resistance: ~12 MΩ). Signals were pre-amplified using a custom-made amplifier equipped with negative capacitance regulation and low-pass filtered at 3 kHz. Signals were sampled at a frequency of 10 kHz and stored on a computer hard disc for offline analysis (Cambridge Electronic Design, Cambridge, UK).

SW-R in the ventral CA3-CA1. One hour after slice preparation, glass electrodes were placed at stratum pyramidale (SP) of area CA3 and CA1. Data were recorded for 2 min and extracted as MATLAB files to be further analyzed using MATLAB-based functions (MathWorks, Natick, MA) as described previously (Çalışkan et al., 2015b, 2016). In brief, sharp waves (SW) were detected by low-pass filtering the data at 45 Hz (Butterworth, 8th order). The threshold for event detection was set to 2.5 times the standard deviation (SD) of the lowpass-filtered signal. The minimum interval between two subsequent SW was set to 80 ms. Data stretches of 125 ms centered to the maximum of the sharp wave event were stored for further analysis. To analyze the area under the curve of SW, the points crossing the mean of the data were used as the start and the end point of SW. The SW area was measured using trapezoidal numerical integration of low pass-filtered data. To isolate the ripples, the raw data were band-pass filtered at 120-300 Hz (Butterworth, 8th order). Data stretches of 15 ms before and 10 ms after the maximum of SW event (25 ms) were stored for further analysis. The threshold for ripple detection was set to 3 times SD of the band-pass filtered signal. To analyze the ripple amplitude, triple-point-minimax-determination was used. If the difference between falling and rising component of a ripple was higher than 75 %, ripples were discarded from the analysis. Frequencies were calculated only from subsequent ripples.

Carbachol-induced gamma oscillations in the ventral CA3-CA1. Carbachol (CBh, 5 μM) was diluted freshly prior to the experiment and applied via continuous bath perfusion. Prior to perfusion of slices with CBh, the temperature of the recording chamber was increased to 35°C. After 50-70 min perfusion of CBh, glass electrodes were placed at stratum pyramidale (SP) of area CA3 and CA1. Gamma oscillations were analyzed using custom-made spike2 (version 8) scripts (Cambridge Electronic Design, Cambridge, UK). For this analysis, power spectra were generated from 2 min records by Fast Fourier Transformation using a frequency resolution of 0.8192 Hz. Three parameters of the power spectra were analyzed for each data set: (1) Peak frequency (Hz): the frequency value at the maximum power value. (2) Peak power (mV^2): the power value at the maximum power. (3) Integrated power (mV^2): the sum of power from 20 to 60 Hz. As a cut off criteria, we did not include the slices with peak powers lower than 0.00001 mV^2 and peak frequencies lower than 20 Hz. For the autocorrelation analysis two min files were extracted from each recording and auto-correlograms were calculated using Spike2 (version 8) software. The amplitude of the 2nd positive peak of auto-correlations was further used for the statistical analysis. For

the cross-correlation analysis of CA3 and CA1 gamma oscillations the 1st positive peak of the cross-correlogram was used for the statistical comparison.

Behavioral analysis

All behavior experiments were performed between 10 am and 5 pm. If more than one behavioral experiment was going to be performed with the same mice, testing began with the least stress and anxiety inducing and ended with the most stressful.

The ***home cage activity*** of mice was monitored using an infrared detection system (HCA 10-V2.1, Coulbourn Instr., Holliston, MA, USA) for 120 h, where activity was recorded in 5 min bins and analyzed per hour (Albrecht et al., 2013b). The ***open field*** test was performed in a 50 cm x 50 cm x 30 cm arena on two consecutive days, 24 h apart, with each one 20 min session. The experimental room was illuminated with red light (<10 lux). The distance travelled in the maze and exploratory patterns were tracked using video surveillance and analyzed with AnyMaze software (Stoelting Co., Wood Dale, IL, USA) (Muller et al., 2014). Data were analyzed in 5-min bins for both days. The ***elevated plus maze*** test was performed on a maze consisting of two closed and two open arms 35 cm long each, 5 cm wide and 40 cm elevated from the ground. Mice were tested during the dark phase, between 12 and 4 pm. To start the experiment animals were placed in the center of the maze and exploratory behavior was tracked for 5 min under low light conditions (10 Lux). Entries and time spent in the open and closed arms were tracked and analyzed with AnyMaze software (Rehberg et al., 2010). The ***light/dark transition test*** apparatus consisted of two compartments (each 19 cm x 21 cm x 20 cm) separated with a 4 cm x 4 cm opening: the light compartment (100 lux) and dark compartment (<1 lux). Mice were introduced to the light compartment facing away from the opening and tested for 5 min in the maze. The time spent in each compartment and the transitions between compartments were recorded by a photo-beam detection system (TSE, Bad Homburg, Germany) (Albrecht et al., 2013a, 2013b). ***Active avoidance*** task in a shuttle box (36 cm x 21 cm x 20 cm) with two equal size compartments separated with an opening (4 cm x 4 cm) (TSE, Bad Homburg, Germany) and a photo-beam detection system was used to assess the position of the mouse in the box and record the activity. Training was done over a period of 5 days, with 50 trials per day. Each session started with a 3-min habituation phase. Tones (10 kHz, 65 dB) were used as conditioned stimuli (CS) and were presented for an initial 5 s without foot shock reinforcement, followed by co-presentation with a foot shock (0.40 mA for max 10 s, followed by 0.60 mA for max 5 s), which was immediately stopped once the mouse shuttled to the other compartment. The inter trial interval was set to 20 s. Trials were considered successful if the animal shuttled before the foot shock onset. ***Social memory*** was tested in a 3-chamber social interaction setup with compartments that measure 20 cm x 40 cm each and Plexiglas walls with an open middle section separating the three chambers without restricting access to any compartment (Albrecht and Stork, 2012). The test was performed under dim light conditions (35 lux) in three stages, 5 min each, by placing the subject mouse into the middle compartment and allowing the mouse to explore all three chambers of the setup freely. Mice were tested between 1-5 pm, during the dark phase. Two identical, wire tube-like containers that are large enough to hold a single mouse (8 cm in diameter) were placed inside the setup vertically, one in each side chamber. In the first stage (habituation), both of these wire containers were kept empty as the subject mouse explored the setup and the interaction time with each of the tubes was scored. In the second part (sociability test), a male, age-matched, wild-type (C57BL/6JBomTac - M&B Taconic, Germany) partner mouse was placed in one of the wire tubes in random and the interaction time of the subject mouse with the partner vis-a-vis the empty container has been scored. In the last part (social novelty preference test) of the experiment, a second wild-type partner mouse (novel) occupied the previously empty wire container as the interaction time with the already familiarized partner against the novel partner has been scored. AnyMaze software (Stoelting Co., Wood Dale, IL, USA) was used for the tracking of the subject mouse and scoring of interaction times. A place learning protocol in the ***water-cross-maze*** was done (Kleinknecht et al., 2012): the test was performed in a 23°C water filled maze with spatial cues placed around it. Mice went through training to find the hidden platform placed in the one arm of the maze for 5 days, 6 trials per day. The opposite arm of the starting arm was blocked, and mice had the choice to turn left or right to find the platform depending on the spatial cues. A score 1 was given as accurate, when the mouse swam directly to the platform without entering or turning to the wrong arm. Mice with 83.3% or higher accuracy on the fifth day of training continued with the reversal-learning test where the platform was in the opposite arm. Reversal learning also took 5 days, 6 trials per day. Accuracy and latency to find the platform were determined by the experimenter, who was blind with respect to genotype in all experiments.

QUANTIFICATION AND STATISTICAL ANALYSIS

TG mice were always analyzed in comparison to their WT littermates, derived from several (at least 3) independent litters. Experimental procedures and quantification were carried out by an experimenter who was blind with respect to animal genotype. Sample sizes were estimated using the program G*Power ($\alpha = 0.05$, $\beta = 0.8$, strong effects). Prism (GraphPad Software, Inc.) and SigmaPlot (Systat Software Inc.) were used for statistical analyses and data presentation. Data were evaluated for normality using Shapiro-Wilk Test and equal variance before group comparison. For qPCR, Timm's staining, MF-LTP, and behavior data Student's *t*-test, Mann-Whitney *U*-test, one-way-ANOVA or repeated measures (RM) two-way-ANOVA were used. For post-hoc comparisons Fisher's LSD test was performed when applicable. p values <0.05 were considered significant. N values indicate number of animals, n is used to indicate number of samples (slices for electrophysiology). Data are generally presented as mean $\pm$ SEM. The corresponding Results section reports on values and statistical analysis of experimental data not included in the figures and figure legends.